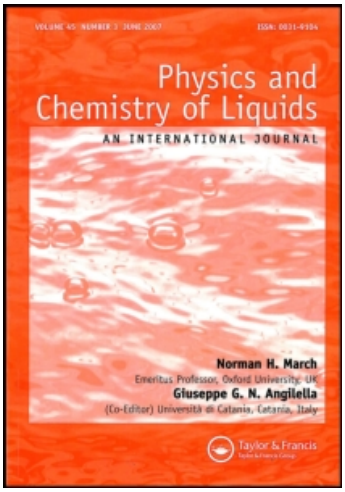

Physics and Chemistry of Liquids

Publication details, including instructions for authors and subscription information:
http://www.informaworld.com/smpp/title~content=t713646857

Review: Water at ions, biomolecules and charged surfaces

I. Danielewicz-Ferchmin[a]; A. R. Ferchmin[b]
[a] Faculty of Physics, Adam Mickiewicz University, PL-61-614 Poznań, Poland [b] Institute of Molecular Physics, Polish Academy of Sciences, PL-60-179 Poznań, Poland

To cite this Article Danielewicz-Ferchmin, I. and Ferchmin, A. R.(2004) 'Review: Water at ions, biomolecules and charged surfaces', Physics and Chemistry of Liquids, 42: 1, 1 — 36
To link to this Article: DOI: 10.1080/0031910031000120621
URL: http://dx.doi.org/10.1080/0031910031000120621

Physics and Chemistry of Liquids
Vol. 42, No. 1, February 2004, pp. 1–36

Taylor & Francis
Taylor & Francis Group

Review

WATER AT IONS, BIOMOLECULES AND CHARGED SURFACES

I. DANIELEWICZ-FERCHMIN[a] and A.R. FERCHMIN[b,*]

[a]*Faculty of Physics, Adam Mickiewicz University, ul. Umultowska 85, PL-61-614 Poznań, Poland;*
[b]*Institute of Molecular Physics, Polish Academy of Sciences, ul. M. Smoluchowskiego 17, PL-60-179 Poznań, Poland*

(Received 15 March 2003)

Research that has led to writing the equation of state of an open system containing water in an electric field and to prediction of a related phase transition at the same time as its experimental discovery was announced, is reviewed. X-ray and neutron scattering, dielectric, picosecond photothermal/photoacoustic, thermal and electrochemical measurements contribute to our understanding of these phenomena and are discussed from a unique point of view. New theoretical results are presented and compared with experiment.

Keywords: Phase transition; Equation of state; Density; Electrostriction; Dielectric saturation; Electrolyte; Protein; Hydration shell

CONTENTS

1 INTRODUCTION 2
2 WATER IN OPEN SYSTEMS – RESPONSE TO HIGH ELECTRIC FIELD 3
2.1 The Equilibrium Condition as a Basis for Writing the Equation of State 3
2.2 A Statistical Model of Water Permittivity 4
2.3 The Equation of State of H_2O Expressed in the Variables T, Π, E 11
2.4 Change of Entropy ΔS in the Field E: Electrocaloric Effect 15
2.5 Phase Transition in H_2O Induced by Electrostriction Pressure Π 17
3 COMPARISON WITH EXPERIMENT 19
3.1 An Overall Picture of Water in Electric Field $E > 10^8$ V/m 19
3.2 The Helmholtz Layer 20
3.3 Hydration Shells of Ions 22
3.4 Protein Hydration in Solution 29
4 REMARKS ON THE METHOD 31
5 SOME PERSPECTIVES 32
6 CONCLUSION 32
Nomenclature 33
References 34

*Corresponding author. E-mail: arfer@ifmpan.poznan.pl

ISSN 0031-9104 print: ISSN 1029-0451 online
DOI: 10.1080/0031910031000120621

1. INTRODUCTION

For more than a decade there has been growing experimental evidence of phase transitions of molecular layers of liquid water to dense solid phases under the action of a strong electric field at ambient conditions [1,2]. To our knowledge, the first evidence of transitions of liquid water to possibly different phases in high electric fields at ambient conditions is due to Kasinski *et al.* [1]. By optical excitation of surface acoustics they have found "evidence for a liquid–solid phase transition at the highly polar TiO_2 surface, i.e., a rigid layer of H_2O at the TiO_2 interface". This line of research was later followed by Harata *et al.* [3] who performed hypersonic investigation of picosecond photothermal/photoacoustic phenomena at the Au–aqueous electrolyte interface. Their results obtained by transient grating spectroscopy methods were interpreted in terms of potential-dependent (actually field-dependent) enhancement of water density. Very recently, by *off-specular* X-ray scattering technique, it was possible to reveal phase transitions in water layers compressed vertically to the surface of an RuO_2 charged electrode [2] by fields of the order of $10^9\,\mathrm{V\,m^{-1}}$. This observation had been preceded by *specular* X-ray investigation [4,5] of water at a charged Ag electrode, which revealed water layers polarized and compressed to a density as high as twice the normal one. The latter observation has been explained qualitatively by the authors [4,5] and later quantitatively by the authors of this work [6] as due to electrostriction. Note that field strengths leading to high density of H_2O can be found also in the first hydration shells of some ions [4]; hence, the latter problem has been treated on an equal footing [7] with that of polar interfaces. An enhanced density was also observed in the vicinity of protein molecules [8]. These observations gave an incentive to a theoretical approach to the problem of phase transitions in water under the influence of electric field. It comes out from the nature of the present problem, which involves electrostriction [4,5], that it should be treated in terms of open systems [6,9].

In this article, on the basis of the equation of state written for an open system of H_2O molecules in a local electric field, we review the problem of phase transition in the field from a unique point of view. Related experiments belong to different domains of investigation such as laser irradiation and detection, X-ray and neutron scattering, electrochemistry and physical chemistry of biomolecules. Within the same approach, we deal with problems of dielectric saturation (ϵ), huge electrostriction (d), large electrocaloric effect (ΔQ), properties of molecular H_2O layers at charged electrodes and hydration of ions and protein molecules.

The rest of the article is organized as follows. The next section is concerned with the formulation of the condition for thermodynamic equilibrium between parts of the system of H_2O molecules within the electric field and outside it. It serves as a basis for writing the equation of state. This is done with the help of a statistical model describing the response of H_2O electric dipole moments to the field. Literature data on isotherms under high pressure (in no field) have been applied. This model enables one to calculate, for instance, the changes in entropy (electrocaloric effect). Discussion of the entropy changes and the equation of state leads to a prediction of a phase transition due to the action of electrostriction pressure. The following section, devoted to a comparison with experiment, begins with a presentation of an overall picture of hydration shells of ions and molecular layers at charged electrodes in terms of two different phases. This is confronted with results of various experiments: X-ray and neutron scattering, latent heat at the transition and optical excitation of

surface acoustic modes. Also, the problems of hydration of proteins in solutions are discussed. At last, we include remarks on the theoretical methods applied, draw some perspectives for further investigation and end with conclusions.

2. WATER IN OPEN SYSTEMS – RESPONSE TO HIGH ELECTRIC FIELD

2.1 The Equilibrium Condition as a Basis for Writing the Equation of State

Within the present approach we consider the water placed in a local high electric field (Fig. 1, subsystem *i*) that is the water in the double layers at charged surfaces and that in hydration shells of ions (cf. [6,7] and references therein). It forms a common system with the remaining water (Fig. 1, subsystem *o*) localized in a weak field or outside the field. The thermodynamic law describing the state of the whole system is the equilibrium condition with respect to the mass transport between the regions within and outside the field. It follows from the condition of equality of the chemical potentials ζ (cf. [10,11]):

$$\zeta^i = \zeta^o. \tag{1}$$

For the fields of the strengths $E > 10^9\,\mathrm{V\,m^{-1}}$ the mean cosine $\langle\cos\theta\rangle$ is > 0.99 [12], which means that very strong electric fields produce a *dielectric saturation phenomenon*. Models of the dipole orientation contribution and effects of dielectric saturation were already earlier treated in the context of metal–electrolyte interface ([13], p. 119 therein) and in the context of the hydration shells of ions ([14], p. 142 therein). The subsystem *i* (Fig. 1) represents an open system: the number of dipolar molecules vary as the dipoles are pulled from the subsystem denoted by *o*, exterior to the field into the field. This is accompanied by a *huge electrostriction*. The effect of striction corresponds to that of local pressures of the order of gigapascals and leads to enhancement of the local relative density *d* of H_2O. The application of an electric field $E > 10^9\,\mathrm{V\,m^{-1}}$ to H_2O also produces a *large electrocaloric effect*. The corresponding change in the energy of the system is compensated in isothermal conditions by a heat flow from outside. The large isothermal electrocaloric effect must be taken into account, e.g., in the energy balance during dissolution of salts in water [15]. We shall present a theoretical evidence that H_2O at ambient conditions in a field of a strength taking the values from the range $0.77 < E < 1.36$ ($10^9\,\mathrm{V\,m^{-1}}$) (cf. Table I) undergoes a phase transition to a dense and orientationally ordered phase of H_2O at a transition value $\Pi_t = 0.2\,\mathrm{GPa}$ of the local electrostriction pressure [16]. The transition is accompanied by a latent heat as well as discontinuities in entropy and electric field. Hence, one can expect the appearance of a dense and

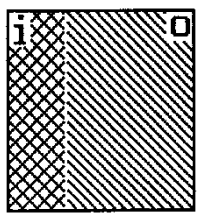

FIGURE 1 A thermodynamic system divided into subsystems: *i* situated in a high electric field *E* and *o* in the field $E \to 0$, schematically.

TABLE I Lower and upper values of the electric field strength E, change in entropy $-\Delta S$, permittivity ϵ, reduced distance x and free charge surface density σ_0 at discontinuity

E (10^9 V m^{-1})	0.77	1.36
$-\Delta S$ (J mole^{-1} K^{-1})	1.90	0.97
ϵ	38	22.8
x (10^{-10} m)	2.217	2.154
σ_0 (10^{-3} C m^{-2})	6.8	12.0

orientationally ordered phase, which will be called phase A of H_2O for fields of strength $E > 1.36$ (10^9 V m^{-1}). Note that such fields exist also the in first hydration shells of ions with reduced radii $x_1 < 2.154$ Å and in Helmholtz layers at surfaces with surface charge density $\sigma_0 > 0.012$ C m^{-2} (cf. Table I). The condition $x_1 < 2.154$ Å is fulfilled for triply and quadruply charged ions, for the majority of doubly charged ions and for Li^+. As we shall see, H_2O in the first hydration shells of these ions can be interpreted in the framework of our approach as belonging to a dense and orientationally ordered phase A. The surface charge density $\sigma_0 > 0.012$ C m^{-2} is encountered in X-ray investigation of charged solid–water interface [2,4,5]. The σ_0 value in [1] for the TiO_2–water interface should also fulfill this inequality.

A high electric field E performs a work W by reorienting a water molecule placed in it. At the same time, the chemical potential is reduced by ζ_W with respect to that of a molecule outside the field. To attain an equilibrium, the chemical potential gradient thus created induces the pull of the dipoles into the field. We are interested in a new equilibrium state with water density increased in the high field (say, in the first hydration shell of the ion, or in a double layer) due to this process. The work L related to water compression in the field – the electrostriction work – enhances the chemical potential of water by ζ_L. After reaching the equilibrium, the latter compensates the negative increment ζ_W:

$$-\zeta_W = \zeta_L. \tag{2}$$

With the electrostriction effect as a connection between the mechanical (mass density) and electric (electric field strength) quantities, and the experimental X-ray data of [4,5] at hand, there arises a possibility to find the electric characteristics of the first layer of molecules (and possibly ions) at the electrode. This has been done in [17] profiting from the fact that the mass density – surface charge density relationship was derived previously in [6].

2.2 A Statistical Model of Water Permittivity

To relate the electric permittivity ϵ with the dipole moment μ of a molecule one applies a statistical mechanical calculation leading to $\langle \cos\theta \rangle$ – the mean cosine [18,19] of the angle θ. Usually, $\langle \cos\theta \rangle$ is expressed by the Langevin function [20,21], which leads to correct predictions of the dielectric constant values for polar liquids with no hydrogen bonds. In the linear approximation,

$$\langle \cos\theta \rangle = \frac{\mu E_{\text{on}}}{3kT}, \tag{3}$$

where E_{on} is the Onsager local field [18,19]. The Onsager field approximation [18,19] is up to the present [22] considered as one of the best in application to classical dipole systems. Its application, as will become clear in the following, is by no means limited to uniform weak fields, contrary to a remark by Sandberg and Edholm [23]. Let us also point out that there exist microscopic approaches to the Onsager field problem based on statistical mechanics [24,25] not invoking the notion of a continuum. This is also the case in the domain of magnetism ([26] and references therein).

Equation (3) for $\langle \cos\theta \rangle$ does not hold for liquids with hydrogen bonds. For water, at ambient conditions, to achieve agreement with experiment, $\langle \cos\theta \rangle$ has been expressed [6] by a Brillouin function [20,21]

$$B_2(\Xi) = \tanh(\Xi), \tag{4}$$

$$\Xi = \frac{\mu E_{on}}{kT} \tag{5}$$

corresponding to two admitted orientations of the dipole moment and then, in the linear approximation [27,28], $\langle \cos\theta \rangle = \mu E_{on}/kT = \Xi$. The plot of Fig. 2 illustrates the different behavior of hydrogen-bonded and other liquids. It is replotted from Cole [29] with a straight line added, marked ONSAGER(2) to stress the two

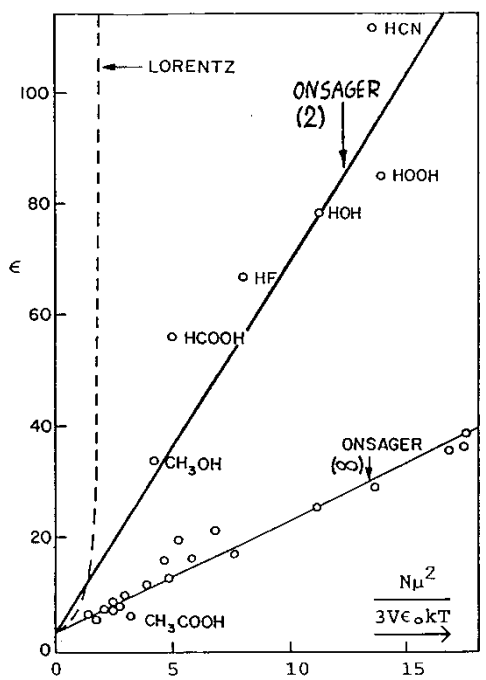

FIGURE 2 Electric permittivity ϵ of dipolar liquids as a function of $N\mu^2/(3V\epsilon_0 kT)$. Circles denote experimental data, the straight lines – values of ε calculated on the basis of the Onsager theoretical model: Onsager(∞) – calculated on applying Langevin function (with any orientation of dipole moment possible). Onsager(2) – calculated an applying the Brillouin function for only two possible orientations of dipole moment (see text). After [29] with the straight line denoted Onsager(2) added by one of the present authors (cf. [12]).

allowed orientations of the dipole when calculating $\langle \cos\theta \rangle$ within the Onsager model, but with the Brillouin function B_2 for hydrogen-bonded liquids instead of the usual Langevin function. The latter case results in the straight line marked ONSAGER(∞) to stress the infinite number of allowed dipole orientations which applies to the ordinary dipolar liquids. Figure 2 makes it clear that the duly modified Onsager model provides a good description of the dielectric properties of liquids associated by hydrogen bonds. The external field E is related to E_{on} as follows (cf. [19], Eq. (5.52), p. 175 therein):

$$E_{\text{on}} = \frac{\epsilon (n^2 + 2)}{2\epsilon + n^2} E. \tag{6}$$

For the flat geometry of the spatial distribution of the charges generating the field E we have

$$E = \frac{\sigma}{\epsilon\epsilon_0} \quad \text{and} \quad \sigma = \epsilon\sigma_0. \tag{7}$$

Substituting Eq. (7) to Eq. (6) we get

$$E_{\text{on}} = \frac{n^2 + 2}{\epsilon_0(2\epsilon + n^2)} \sigma. \tag{8}$$

Equation (8) can be applied to different geometries of the spatial charge distribution, which will be encountered in the following, by a proper definition of σ.

For the spherical geometry E represents the Coulomb field

$$E = \frac{q}{4\pi\epsilon\epsilon_0 x^2}, \tag{9}$$

where q is the elementary charge and we have

$$\sigma = \frac{q}{4\pi x^2}. \tag{10}$$

A flat geometry is represented by the shape of the electrode [6]. The spherical geometry is encountered in the ion hydration problem [7]. Equation (9) implies infinite dilution – the field strength depends only on the distance from the center of a single ion.

In the framework of such an approach the reorientations of dipoles responsible for the high dielectric constant of water and ice, can be thought as due to simultaneous shifts of the proton positions, as first suggested by Pauling [28]. The two possible orientations ($I = 2$) of water molecules linked by hydrogen bonds at room temperature are illustrated, very schematically, in Fig. 3(a). At room temperature, the hydrogen bond energy (20–25 kJ mole^{-1}) exceeds the thermal energy RT (~ 2.5 kJ mole^{-1}) by a factor of about ten. Hence, the very concept of two possible orientations of water dipoles at ambient conditions seems to be justified. It is also corroborated by the agreement of theoretical predictions [30] of the nonlinear dielectric effect in water with experiment [31,32]. At very high temperatures, in which the thermal energy becomes comparable to the hydrogen bond energy ($T \sim 3000$ K, $RT \sim 25$ kJ mole^{-1}) the hydrogen bonds should be broken (cf. Fig. 3b) and dipoles could rotate freely ($I = \infty$), which induces a behavior

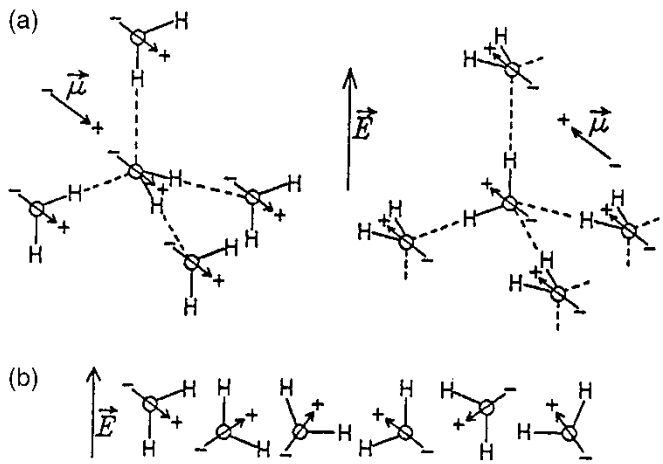

FIGURE 3 (a) Water molecules (at ambient temperature) linked with hydrogen bonds, schematically. Arrows mark their dipole moments μ. Reorientation of the dipole moments μ is due to the simultaneous shifts in the proton positions. The figure illustrates the fact that in such systems only two orientations of a dipole moment are allowed ($I=2$). (b) Freely rotating water molecules at very high temperatures (see text), schematically. Their dipole moments μ can take arbitrary orientations in space ($I=\infty$).

described by the Langevin function $L(\Xi)$. In this context it is natural to seek for an interpolation scheme between the two extremes of $\tanh \Xi$, corresponding to $I=2$, and $L(\Xi)$, corresponding to $I=\infty$, which represent the upper and lower bound of $\langle \cos\theta \rangle$, respectively. It is conceivable that in the intermediate temperature range part of hydrogen bonds are disrupted, which can be thought as leading to an intermediate number I of probable directions of the dipole moments lying between the two extremes: $2 < I < \infty$.

The value of $\langle \cos\theta \rangle$ for an arbitrary number I of orientations of a dipole is expressed by the Brillouin function [20, 21]

$$B_I(\Xi) = \frac{I}{I-1} \coth \frac{I\Xi}{I-1} - \frac{1}{I-1} \coth \frac{\Xi}{I-1}, \tag{11}$$

where Ξ is defined in Eq. (5). The Brillouin functions are known in the physics of magnetism, similarly as the Langevin function $L(\Xi)$ introduced for the first time in the theory of paramagnetism. The form of $L(\Xi)$ is obtained from the Brillouin function $B_I(\Xi)$ in the limit $I \to \infty$. For small values of the argument Ξ the function $B_I(\Xi)$ can be expanded into the power series:

$$B_I(\Xi) = \frac{I+1}{3(I-1)} \Xi - \frac{I^4-1}{45(I-1)^4} \Xi^3 + \cdots \equiv b(I)\Xi - c(I)\Xi^3 + \cdots \tag{12}$$

The coefficient $b(I)$ and the mean number of orientations I of the dipole moment are interrelated as (cf. Eq. (12))

$$b(I) = \frac{I+1}{3(I-1)}, \tag{13}$$

or inversely

$$I = \frac{3b+1}{3b-1}. \tag{14}$$

The relation between the permittivity ϵ and the electric field strength is, according to the Onsager field model expressed as (cf. [33]):

$$\frac{\epsilon - n^2}{\epsilon} = \frac{NB}{\sigma V}\langle\cos\theta\rangle, \tag{15}$$

where

$$B = \frac{\mu(n^2+2)}{3} = 7.59 \times 10^{-30}\,\mathrm{C\,m}, \tag{16}$$

$$\langle\cos\theta\rangle = B_I(\Xi) \tag{17}$$

and for $I = 2$

$$\langle\cos\theta\rangle = \tanh(\Xi). \tag{18}$$

From Eqs. (8) and (5)

$$\Xi = \frac{\sigma A}{Tg}, \tag{19}$$

where

$$g = \left(\epsilon + \frac{n^2}{2}\right), \tag{20}$$

$$A = \frac{\mu(n^2+2)}{2k\epsilon_0} = 9.32 \times 10^4\,\mathrm{K\,C^{-1}\,m^2}. \tag{21}$$

For $I = 2$, omitting the notation (Eqs. (16) and (21)) aimed at simplifying the formula and taking into account Eqs. (18) and (19), Eq. (15) and can also be written as:

$$\frac{\epsilon - n^2}{\epsilon} = \frac{\mu(n^2+2)N}{3\epsilon\epsilon_0 EV}\tanh\frac{\mu\epsilon(n^2+2)E}{2kT(\epsilon + n^2/2)}. \tag{22}$$

Permittivity ϵ of H_2O as a function of the reduced distance x is plotted in Fig. 4 for $T = 293\,\mathrm{K}$. The supplementary abscissa axes show field strength E and surface charge density σ_0 corresponding to the related values of x (cf. Eqs. (7) and (9)). Yet another relation of the permittivity as a function of σ is given in Fig. 5.

Relations $\epsilon(E)$ leading to plots similar to those shown in Figs. 4 and 5 have been known in literature for a long time: Grahame relation [34,35] and that proposed by Glueckauf [14,36]. However, it should be stressed that both formulas: that due to Grahame as well as that proposed by Glueckauf do contain adjustable parameters

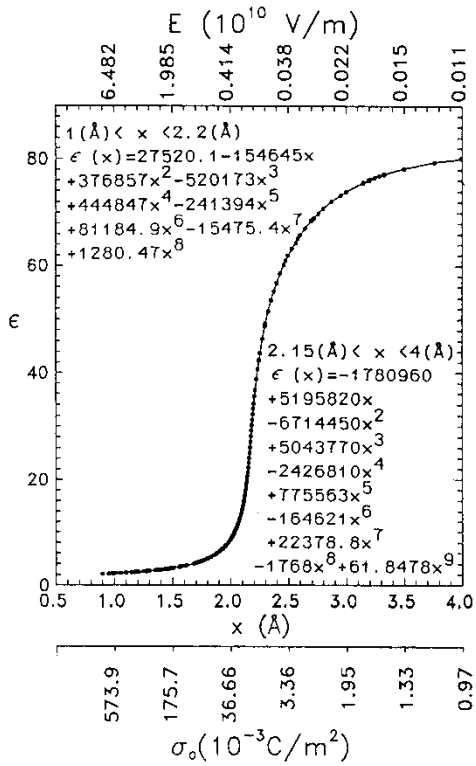

FIGURE 4 Permittivity ϵ as a function of the reduced distance x from the ion. 164 points marked represent pairs (ϵ, x) fulfilling Eq. (15) at $T = 293\,\mathrm{K}$. Two different fitting polynomials: one for the range $1 < x < 2.2$ Å and another one for the range $2.15 < x < 4$ Å are explicitly written. The supplementary abscissa axes show field strength E and surface charge density σ_0 corresponding to the related values of x.

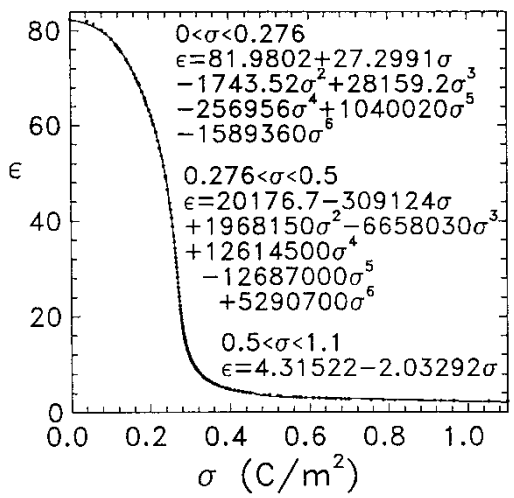

FIGURE 5 Permittivity ϵ as a function of the surface charge density σ. The points marked represent pairs (ϵ, σ) fulfilling Eq. (15) at $T = 293\,\mathrm{K}$. Two different fitting polynomials of 6th order in σ: one for the range $0 < \sigma < 0.276\,(\mathrm{C\,m^{-2}})$ and another one for the range $0.276 < \sigma < 0.5\,(\mathrm{C\,m^{-2}})$ are explicitly written. A linear fit is shown for the range $0.5 < \sigma < 1.1\,(\mathrm{C\,m^{-2}})$.

that affect the dependence of permittivity ϵ on the number density N/V and absolute temperature T. By contrast, our Eq. (22) does not contain adjustable parameters. It is a formula expressing the dependence of permittivity ϵ *explicitly* on electric field strength E (or reduced distance x), number density N/V and absolute temperature T. Thus, it can serve as a basis to calculate the derivatives $(\partial\epsilon/\partial N)$ (needed to find the change in chemical potential ζ_W due to electric field, and further on – the electrostriction) and $(\partial\epsilon/\partial T)$ (needed to find the entropy and further on – the value of the electrocaloric effect). To our knowledge, apart from the Eyring's theory [27], this is the only parameter-free formula of this kind in literature. The possibility to calculate these derivatives on the basis of Eq. (22) enables one to further calculate the electrostriction pressure and entropy needed to find the value of the electrocaloric effect, with no fitting at all.

The numerical value $b(I)=b(\infty)=1/3$, in the theory of permittivity based on the Onsager model of local field E_{on}, follows from the assumption that all orientations of the dipoles are allowed ($I=\infty$), and one arrives at the expression for the dielectric constant (cf. [19], Eq. (5.67), p. 178 therein):

$$\frac{3(\epsilon-n^2)(2\epsilon+n^2)}{\epsilon(n^2+2)^2}=\frac{1}{3}\frac{\mu^2 N}{\epsilon_0 VkT}, \tag{23}$$

where $1/3=b(\infty)$. According to our proposed interpolation scheme [33], for small electric fields, starting from the Brillouin function instead of the Langevin function, one arrives (cf. Eq. (12)) at an analogous expression for the dielectric permittivity ϵ containing the factor $b(I)$ instead of 1/3 present in Eq. (23):

$$\frac{3(\epsilon-n^2)(2\epsilon+n^2)}{\epsilon(n^2+2)^2}=b(I)\frac{\mu^2 N}{\epsilon_0 VkT}, \tag{24}$$

The numerical value of $b(I)$ can readily be found from Eq. (24) provided that the other quantities, and in particular the dielectric constant ϵ at a given temperature T and number density (depending on pressure P), are known from experiment. Note that $b(I)$ must fulfill the inequality:

$$\frac{1}{3}\leq b(I)\leq 1. \tag{25}$$

The empirical fact that the low-field dielectric constant data do indeed lead to the values for the coefficient $b(I)$ fulfilling the inequality (25) confirms the possibility of application of our interpolation scheme. If the experimental data are such that $b(I)$ bears values leading to noninteger values of I (cf. Eq. (14)), the function $B_I(\Xi)$ should be treated as *defined* by Eq. (11). In [33] we have given $b(I)$ values for $293<T\leq 573\,\text{K}$, which enabled us to find a correlation between the temperatures at which destroyed hydration structures [37] and the melting line of H_2O were observed. The idea of varying the mean number of orientations of dipole moments of H_2O molecules with temperature, applied in [33] was developed by Eyring [27] in the context of a mixture (two species) model of water. The concept of introducing the factor $b(I)$ as a

parameter has been in another context proposed in [38] in connection to the permittivity of alcohols in nonpolar solvents.

In the following, we shall write the thermodynamic equation of state and calculate changes in entropy as well as the electrocaloric effect under the action of an electric field. To this purpose, we shall need the derivatives $(\partial\sigma/\partial\epsilon)$, $(\partial\epsilon/\partial N)$ and $(\partial\epsilon/\partial T)$, which will be obtained from Eq. (22) in a way similar to that given in [6,15].

$$\left(\frac{\partial\sigma}{\partial\epsilon}\right)_{\zeta_L} = \frac{\sigma^2 V(n^2g^2 + (N^oAB\epsilon^2/TV(\cosh\Xi)^2)}{N^oB\epsilon^2 g(A\sigma/T(\cos\mathrm{h}\Xi)^2 - g\tanh\Xi)} \tag{26}$$

and

$$\left(\frac{\partial\epsilon}{\partial N}\right)_{y} = \frac{B\epsilon^2 g^2\tanh\Xi}{V\sigma(N^oAB\epsilon^2/TV(\cosh\Xi)^2 + n^2g^2)}. \tag{27}$$

From Eq. (22) expressing the permittivity ϵ as a function of temperature T, the derivative $\partial\epsilon/\partial T$ is found for various field strengths. After some algebra one arrives at the formula:

$$\left(\frac{\partial\epsilon}{\partial T}\right)_{y,\zeta_L} = \frac{\epsilon - n^2}{T(1-\gamma Vn^2)} + \left(\frac{\partial n}{\partial T}\right)\frac{2n[\epsilon - 1 - \gamma V\epsilon(\epsilon+2)]}{(n^2+2)(1-\gamma Vn^2)} - \alpha_p\frac{\gamma V\epsilon(\epsilon-n^2)}{1-\gamma Vn^2}, \tag{28}$$

where

$$\gamma = \frac{6k\epsilon_0 NTg^2}{[3\sigma V(\epsilon-n^2)]^2 - [N\mu\epsilon(n^2+2)]^2}. \tag{29}$$

σ is given by Eq. (7) and α_p is the thermal expansion coefficient. The values of α_p were taken from [39]; For local electrostriction pressures exceeding 10^8 Pa we applied the values of α_p extrapolated from the data of [39]. The expression $(\partial\epsilon/\partial T)$ obtained from Eq. (28), is shown in Fig. 6 as a function of x. In the following it will be shown that Eq. (28) shall serve as a basis for calculation of entropy changes and the electrocaloric effect. The electrocaloric effect accompanying the changes in entropy of water in the field of ions is the subject of [15], where consistency with the experimental results obtained by electrospray method [40] as well as a density functional calculation [41] is discussed.

2.3 The Equation of State of H_2O Expressed in the Variables T, Π, E

The advantage of an equation of state based on thermodynamic principles is that, by definition, it is applicable to all substances: solid, liquid or gas [42]. Balcerzak derived a rigorous equation of state for a system in *magnetic* field [43] in a way analogous to P, V, T systems dealt with in [42]. In this work, we show that another thermodynamic relationship describing *open* systems in *electric* field leads to an equation of state in T, Π, E variables.

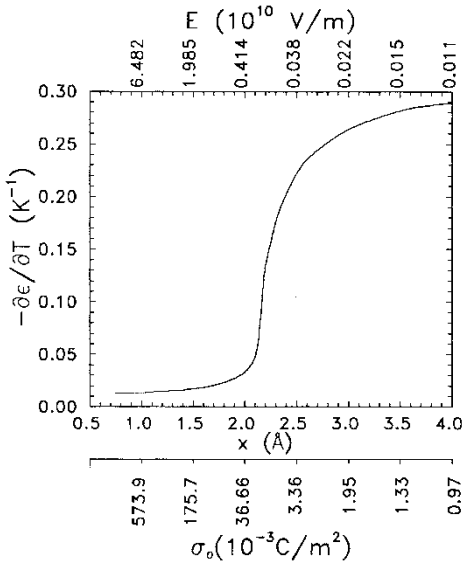

FIGURE 6 Negative derivative $-(\partial\epsilon/\partial T)$ (Eq. (28)) as a function of the reduced distance x from the ion.

We apply this equation to H_2O. More specifically, it shall be demonstrated that a calculation of the work W done by the electric field on a system of dipole moments and the work L related to compression – the electrostriction work – leads to an equation of state expressed in the variables T, Π, E. Equation (43) below (obtained from a detailed form of Eq. (2)) allowing calculation of some parameters of the system from the values of other parameters is the *equation of state*. In [16,44] it is shown that the same equation that relates electric quantities to the mechanical ones implies the existence of a phase transition: normal water $\rightarrow$ compressed H_2O. Let us recall that very recently new X-ray data on the RuO_2–water interface were interpreted as evidence of phase transitions in water monolayers in a high electric field via changes in the chemical potential [2]. A possibility of a phase transition in water at a charged surface has been indicated already in the eighties on the basis of thermal effects accompanying the process of charging a mercury electrode [45].

Having in mind our aim of writing an equation of state, let us first calculate the change in the chemical potential ζ_W (cf. Eq. (2) and [6,7]). The strength of the field is given by Eq. (7). The work W done by the electric field is [6,7]:

$$W = \frac{V}{\epsilon_o}\int_0^y \frac{\sigma}{\epsilon}\,dy, \quad \text{where } y = \sigma\left(1 - \frac{1}{\epsilon}\right). \tag{30}$$

$V = \text{const}$ is the volume of the subsystem i in the field, $V\,dy$ is the increment of the polarization of the subsystem. The increment of the grand potential Ω is:

$$d\Omega = -S\,dT + EV\,dy - N\,\zeta_L. \tag{31}$$

Let us introduce the notation

$$f = \int_0^y \frac{\sigma}{\epsilon}\,dy. \tag{32}$$

The work W performed leads to a change $\Delta\Omega$ in the value of the grand potential Ω of water

$$\Delta\Omega = \frac{V}{\epsilon_0} f. \tag{33}$$

For ζ_W – the change in ζ as a result of the work W one obtains

$$\zeta_W = \left(\frac{\partial\Omega}{\partial N}\right)_{T,V,\zeta_L} \tag{34}$$

The increment

$$\zeta_W = \frac{v^o N^o}{\epsilon_o}\left(\frac{\partial f}{\partial N}\right)_{\zeta_L}. \tag{35}$$

It follows from Eq. (35) that

$$\frac{\zeta_W}{v^o} = \frac{1}{\epsilon_0}\left[\left(\frac{\partial f}{\partial y}\right)\left(\frac{\partial y}{\partial \epsilon}\right)\right]_{\zeta_L} N^o \left(\frac{\partial \epsilon}{\partial N}\right)_y, \tag{36}$$

where

$$\frac{\partial f}{\partial y} = \frac{\sigma}{\epsilon}, \tag{37}$$

and

$$\frac{\partial y}{\partial \epsilon} = \left(\frac{\partial \sigma}{\partial \epsilon}\right)\left(1 - \frac{1}{\epsilon}\right) + \frac{\sigma}{\epsilon^2}. \tag{38}$$

The derivatives $(\partial\sigma/\partial\epsilon)$ and $(\partial\epsilon/\partial N)$ from Eqs. (36) and (38) are given in Eqs. (26) and (27). They can be applied at relatively low temperatures (close to the melting temperature; this includes the ambient temperature). In the hydration shells and double layers the strengths of the electric field are so high that the linear approximation to $\langle\cos\theta\rangle$ is no longer sufficient, and the mean cosine has to be expressed by the full tanh function. The relation between the permittivity ϵ and the electric field strength E is expressed by Eq. (22). Figure 7 shows the values of $-\zeta_W/v^o$ as a function of reduced distance x. In the insert to Fig. 7 there is apparent a kink in the plot at $-\zeta_W/v^o = 0.17 \times 10^9\,\mathrm{J\,m^{-3}}$ near the value of the argument $x = 2.2\,\text{Å}$. In the following it will be argued that this kink is related to a phase transition due to the local electrostriction pressure Π_l.

Let us now turn to the change in the chemical potential ζ_L due to the compression work L which, according to Eq. (2) shall compensate ζ_W. The compression work L is calculated (cf. [6,7]) by integrating the area under the isotherm $V = V(P)$ with P – pressure:

$$L = \int_{P^o}^{P^i} V(P)\, dP. \tag{39}$$

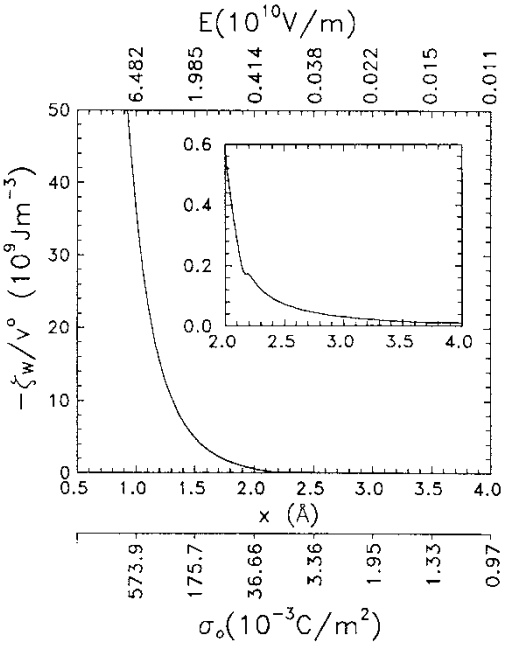

FIGURE 7 Variation in the chemical potential of water molecules ζ_W per volume v^o, due to the work done by the electric field, as a function of the reduced distance x from the centre of an ion. Insert reproduces a part of the plot on an expanded scale. In the insert there is apparent a kink in the plot at $-\zeta_W/v^o = 0.17 \times 10^9\,\mathrm{J\,m^{-3}}$ about the value of the argument $x = 2.2\,\text{Å}$.

The change in the chemical potential ζ_L due to this work is

$$\zeta_L = \frac{\partial}{\partial N}\int_{P^o}^{P_i} V(P)\,dP = \int_{P^o}^{P^i} v(P)\,dP. \tag{40}$$

One can re-write Eq. (2) in the form

$$-\frac{\zeta_W}{v^o} = \frac{\zeta_L}{v^o}, \tag{41}$$

which, taking into account Eqs. (36) and (40), is the same as

$$-\frac{N^o}{\epsilon^o}\left[\left(\frac{\partial f}{\partial y}\right)\left(\frac{\partial y}{\partial \epsilon}\right)\right]_{\zeta_L}\left(\frac{\partial \epsilon}{\partial N}\right)_y = \frac{1}{v^o}\int_{P^o}^{P^i} v(P)\,dP. \tag{42}$$

The integrals on the right hand sides of Eqs. (40) and (42) have been found by substituting the room temperature isotherms of water in the liquid, ice VI and ice VII phases under pressure P in the absence of field [46–48] $V = V(P)$. The upper integral limit (P^i, see Eq. (40)) was matched so as to fulfill Eq. (42). This is equivalent to putting the pressure value P^i in the field equal to the local electrostriction pressure value Π:

$$-\frac{N^o}{\epsilon_o}\left[\left(\frac{\partial f}{\partial y}\right)\left(\frac{\partial y}{\partial \epsilon}\right)\right]_{\zeta_L}\left(\frac{\partial \epsilon}{\partial N}\right)_y = \frac{1}{v^o}\int_{P^o}^{\Pi} v(P)dP, \tag{43}$$

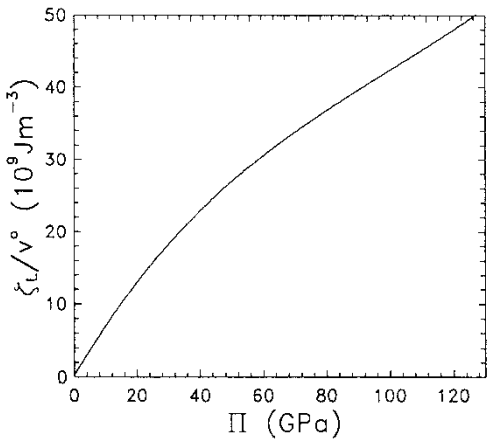

FIGURE 8 Variation in the chemical potential of water molecules ζ_L per volume v^o, due to the work done by the pressure in field-free conditions, as a function of the pressure Π.

In this way, it is admitted that the external pressure applied without electric field would produce water compression comparable to that due to the local electrostriction pressure. It introduces an approximation. Its validity has been positively judged *a posteriori* in [6]. The values of ζ_L/v^o thus found are shown in Fig. 8 as a function of pressure $P^i = \Pi$. Note that a similar approach can be found in literature, e.g., a neutron scattering experiment with isotopic substitution on a 10 M NaOH solution was said to "indicate that ions in aqueous solutions induce a change in water structure equivalent to the application of high pressure" [49].

We have stated that Eq. (43) represents the *equation of state* of H_2O in implicit variables T, Π, and E. Dependence on temperature is present through the relation $\epsilon = \epsilon(T)$ as expressed in Eq. (22) and by introducing of the isotherm $V = V(P)$ for the same temperature T, for which ϵ is calculated into Eq. (43). The electrostriction pressure $\Pi = P^i$. The dependence on the electric field strength E is present in Eq. (22), too. We have dropped the subscripts T and V in Eqs. (26), (27), (35), (36), (42) and (43), keeping in mind that isothermal and constant volume conditions are assumed throughout this work.

2.4 Change of Entropy ΔS in the Field E: Electrocaloric Effect

In addition to electrostriction, the field E induces also a change in the entropy of the system ΔS [10,11,15,19]. The entropy change in the process of water adapting itself to the high field conditions is:

$$\Delta S = \frac{\partial}{\partial T}\Delta\Omega = \frac{V}{\epsilon_0}\left(\frac{\partial f}{\partial T}\right)_{y,\zeta_L} \tag{44}$$

The quantity f (see Eq. (32)) depends on temperature via $\epsilon(T)$. Equation (44) takes the form:

$$\Delta S = \frac{V}{\epsilon_0}\left[\left(\frac{\partial f}{\partial y}\right)\left(\frac{\partial y}{\partial \epsilon}\right)\right]_{\zeta_L}\left(\frac{\partial \epsilon}{\partial T}\right)_{y,\zeta_L} \tag{45}$$

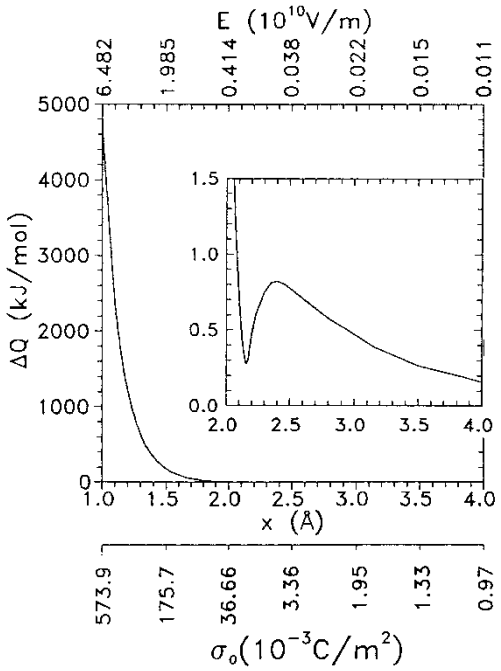

FIGURE 9 Heat ΔQ released as a result of the isothermal electrocaloric effect (Eq. (46)) in water as a function of the reduced distance x from the ion. Insert reproduces a part of the plot on an expanded scale. In the insert there are apparent two extremes about the value of the argument $x \approx 2.2$ Å.

From the latter Eq. (45) it is possible to derive the expression $\Delta Q = T\Delta S$ for the heat absorbed by a dielectric substance during a change in the electric field at a constant temperature:

$$\Delta Q = \frac{TV}{\epsilon_0}\left[\left(\frac{\partial f}{\partial y}\right)\left(\frac{\partial y}{\partial \epsilon}\right)\right]_{\zeta_L}\left(\frac{\partial \epsilon}{\partial T}\right)_{y,\zeta_L} \tag{46}$$

Figure 9 shows ΔQ as a function of the reduced distance x. In the insert to Fig. 9 two extremes are seen in the plot of $\Delta Q(x)$ at about $x \approx 2.2$ Å. We shall see in the following Subsection 2.5 that this anomaly is related to the phase transition. If $(\partial\epsilon/\partial T)_{y,\zeta_L} < 0$, which is usually the case, we have $\Delta Q < 0$ and $\Delta S < 0$. Thus, heat is evolved by the dielectric and given off to the heat bath. At the same time the entropy decreases, due to the ordering of the directions of the dipoles of H_2O molecules in the system by the field. The release of heat by the dielectric as a consequence of a change in the applied field in isothermal conditions is called the *isothermal electrocaloric effect*. The heat due to this effect will be found from Eq. (46). The product of the derivatives:

$$\left[\left(\frac{\partial f}{\partial y}\right)\left(\frac{\partial y}{\partial \epsilon}\right)\right]_{\zeta_L} \tag{47}$$

in known from Eqs. (37) and (38). The derivative $(\partial\epsilon/\partial T)_{y,\zeta_L}$ is calculated from Eq. (28). Locally, neither the derivative $\partial\epsilon/\partial T$ nor ϵ itself are known from experiment. Hence, they are accessible only from a theoretical approach.

2.5 Phase Transition in H_2O Induced by Electrostriction Pressure Π

By definition, a first-order phase transition is characterized by a finite discontinuity in the first derivative of the thermodynamic potential. Here, this is the grand potential Ω (cf. Eq. (31)). Hence, one could expect discontinuities in the electric field strength, entropy and the number N of molecules in a fixed volume V:

$$E = \frac{1}{V}\left(\frac{\partial \Omega}{\partial y}\right)_{V,\zeta_L,T}, \quad -S = \left(\frac{\partial \Omega}{\partial T}\right)_{V,\zeta_L,y}, \quad -N = \left(\frac{\partial \Omega}{\partial \zeta_L}\right)_{V,y,T}. \tag{48}$$

We shall now check if this is the case.

The variable responsible for the transition is the electrostriction pressure Π, related to the remaining state variables by Eq. (43). The relation $E = E(\Pi)$ found from Eq. (43) is shown in Fig. 10. The plot shows that an electric field strength discontinuity occurs at $\Pi_t = 0.208$ GPa (≈ 0.21 GPa), where the subscript t stands for transition. The range of the discontinuity (Fig. 10) is $0.77 < E < 1.36$ ($10^9\,\mathrm{V\,m^{-1}}$). In other words, an increase in the electric field strength E from 0.77 to 1.36 ($10^9\,\mathrm{V\,m^{-1}}$) does not change the value of the electrostriction pressure Π. At Π_t and at a value of E comprised in this range two phases coexist.

From Eqs. (43) and (45) the dependence of entropy change $-\Delta S(\Pi)$ on Π has been obtained and plotted in Fig. 11. A discontinuity in entropy at $\Pi_t = 0.21$ GPa is seen. The range of this discontinuity is: $0.97 < |\Delta S| < 1.9$ ($\mathrm{J\,mole^{-1}\,K^{-1}}$), and it is accompanied by a *latent heat* of $-277\,\mathrm{J\,mole^{-1}}$. On increasing Π from a value equal to atmospheric pressure up to 0.1 GPa ($E = 0.4 \times 10^9\,\mathrm{V\,m^{-1}}$), the entropy of the system of dipoles decreases due to the process of orientational ordering of the dipoles. On the further increase of Π up to the value $\Pi_t = 0.21$ GPa, the entropy increases: the lowering of entropy due to the process of orientational ordering of the dipoles is overwhelmed by its increase. At $\Pi = \Pi_t$ one can notice a discontinuous increase in the entropy due to the coexistence of two phases. On further increasing $\Pi > \Pi_t$ the entropy of a newly created phase decreases.

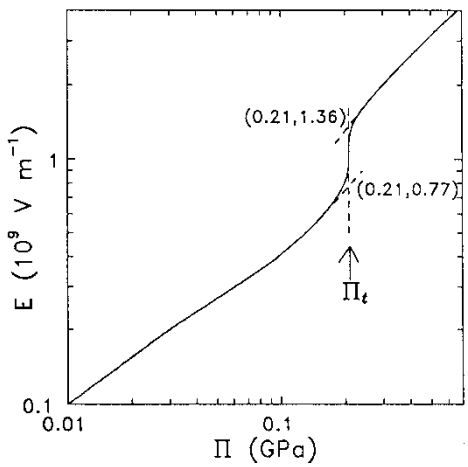

FIGURE 10 Electric field strength $E(\Pi)$ as a function of the electrostriction pressure. The numbers in the brackets mark the coordinates (Π, E) of the lower and upper limits of the discontinuity at the transition value Π_t of the electrostriction pressure.

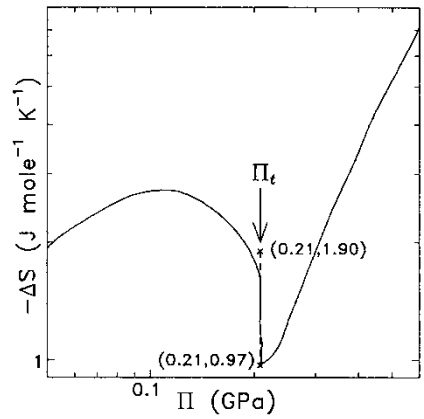

FIGURE 11 Change in entropy $-\Delta S(\Pi)$ as a function of the electrostriction pressure. The numbers in the brackets mark the coordinates $(\Pi, -\Delta S)$ of the lower and upper limits of the discontinuity at the transition value Π_t of the electrostriction pressure.

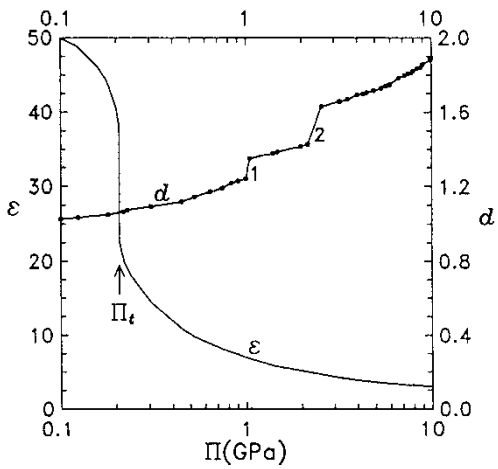

FIGURE 12 Relative mass density $d(P)$ as a function of pressure and permittivity $\epsilon(\Pi)$ as a function of electrostriction pressure. Discontinuity in permittivity ϵ is marked by an arrow, numbers 1 and 2 mark the water $\rightarrow$ ice VI and ice VI $\rightarrow$ ice VII transitions, respectively. The points at the line marked d represent the input data based on the experiment [46–48] (see text).

It is important to note that the value of $\Pi_t = 0.21$ GPa corresponds neither to water $\rightarrow$ ice VI nor ice VI $\rightarrow$ ice VII transitions under external pressure. In Fig. 12, along the line marked d, the $d(P)$ points are shown corresponding to the values of the pressure $\Pi = P^i$ found with the help of Eq. (43) from the experimental data of [46–48]. Between parts of the line with dense points two gaps are seen corresponding to water $\rightarrow$ ice VI (marked by 1, at 1 GPa) and ice VI $\rightarrow$ ice VII (marked by 2, at 2 GPa) transitions under pressures applied in no field ($E = 0$). They are far from the discontinuity in $\epsilon = \epsilon(\Pi_t)$ characteristic of the phase transition found in [16,44]. Hence, the discontinuous phase transition described above is not an artifact resulting from the use of the input data.

For the transition at $\Pi_t = 0.21$ GPa the third quantity in Eq. (48), namely $-N = (\partial\Omega/\partial\zeta_L)$, shows no discontinuity, and hence there is no change in the

specific volume at the transition. This is not an unknown feature in H_2O systems: the transition ice VII $\rightarrow$ ice VIII shows no change in the molar volume: $\Delta v = 0.000 \pm 0.0005\,\mathrm{cm^3\,mole^{-1}}$ (cf. [39], Table 3.6 therein). The latent heat accompanying the transition described in this work: $277\,\mathrm{J\,mole^{-1}}$ is of a comparable order to that found for the transition ice VII $\rightarrow$ ice VIII which amounts to $\Delta Q \approx 1\,\mathrm{kJ\,mole^{-1}}$.

3. COMPARISON WITH EXPERIMENT

3.1 An Overall Picture of Water in Electric Field $E > 10^8\,\mathrm{V/m}$

Figure 13 shows an overall picture of the properties of water emerging from the present calculations, which shall serve to the aim of comparing our predictions with experimental data found in literature. The independent variable in Fig. 13 is x, a quantity related to the electric field strength E (Eq. (9)). This quantity is suitable for discussion of the properties of the hydration shells of ions. The additional abscissa axes are drawn for the surface charge density σ_0, also related to E (Eq. (7)), and the field strength E itself. The variable σ_0 is suitable for a discussion of the properties of a double layer.

By comparing Figs. 7 and 8 and taking into account Eq. (41) as well as our assumption $v^i = v(P^i)$, written now as $v(P^i)/v^o = v^i/v^o (= d^{-1})$, one arrives at a relation (plotted in Fig. 13) between d^{-1} and the field strength E. The predicted values of relative volume, $d^{-1}(x)$, in the range $1 < x < 4$ (Å) ($0.011 < E < 6.482$ ($10^{10}\,\mathrm{V\,m^{-1}}$)), follow a

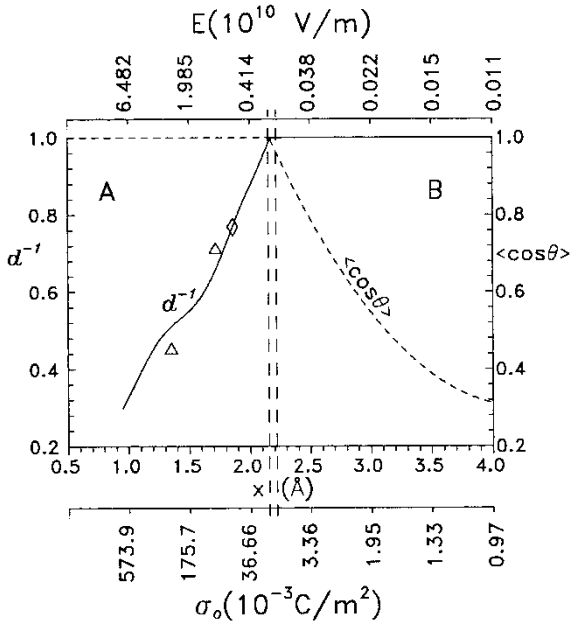

FIGURE 13 Relative volume d^{-1} (left-hand scale, solid line) and mean cosine $\langle \cos\theta \rangle$ of the angle θ (right-hand scale, dashed line) as a function of the reduced distance x. The triangles (Δ) correspond to the density values of H_2O in the first layer of molecules at the electrode found experimentally in [4]. The diamond ($\diamond$) corresponds to the density value in the second layer of molecules (cf. [17]). Two vertical dashed lines are plotted which divide the plot into parts belonging to phases A and B. Between the dashed lines phases A and B coexist. The reduced radii of the first hydration shells of Li^+ and cations doubly, triply and more times charged with the elementary charge fall into the range of the area A. The reduced radii of the second shells of these cations and those of the first shells of singly charged ions fall into the range of the area B.

line. It is characterized by a steep rise of $d^{-1}(x)$ with growing x, followed by a plateau, $d^{-1}(x) = 1$, at $x > 2.217$ Å. At the plateau no distinction can be made between the relative volume of water in the electric field and that of bulk water. The values of $\langle \cos\theta \rangle$ reveal also a plateau at unity, however for $x < 2.154$ Å, and subsequently decrease for $x > 2.217$ Å. The data plotted in Fig. 13 can be divided into two distinct sets corresponding to two areas: A and B, formed due to a division of the plot by two dashed vertical lines at $x = 2.154$ and 2.217 Å (see also Table I for the corresponding value of E and σ_0). For field strengths falling between these two dashed lines the two phases A and B coexist. To the left of these lines, in high fields of strength $E > 1.36 \times 10^9\,\mathrm{V\,m^{-1}}$ one finds the phase A which is dense ($d^{-1} < 1$) and orientationally ordered ($\langle \cos\theta \rangle = 1$). To the right of these lines, in relatively weaker fields $E < 0.77 \times 10^9\,\mathrm{V\,m^{-1}}$ one encounters the phase B of water with only a weak orientational order ($\langle \cos\theta \rangle < 1$) and normal density ($d^{-1} = 1$).

In Fig. 13, one can note no traces of compressed H_2O ($d^{-1} < 1$) for $x > 2.217$ Å; apparently, formation of the phase A is blocked in this range. The value of the electric field such that the energy of H_2O dipole moment in this field equals the hydrogen bond energy W_{HB} (cf. [12]) is $E = 0.29 \times 10^{10}\,\mathrm{V\,m^{-1}}$, the permittivity in this field is $\epsilon = 11.6$, and $x = 2.064$ Å. The latter value of x lies very close to $x = 2.217$ Å at about which d^{-1} begins to drop. One can hypothesize that the structure of untouched hydrogen bonds blocks the pull of additional dipoles into the field up to a threshold value of the energy of dipoles in the field. If the energy of dipoles in the field E approaches W_{HB}, the threshold of a possible breaking of hydrogen bonds is attained, the dipoles become parallel to the field direction ($\langle \cos\theta \rangle = 1$ for $x < 2.154$ Å, Fig. 13) and the blocking of the pull of dipoles into the field is removed.

To pass across a phase transition due to the electrostriction pressure Π_t one should essentially vary electric field strength E in a continuous way. It is feasible by a gradual charging of an electrode immersed in an electrolyte (cf., e.g., the *X-ray scattering experiments* [2,4,5]. A rich series of experimental results can be found in literature on hydration shells of various ions. The fields acting on their hydration shells are $E < 0.77 \times 10^9\,\mathrm{V\,m^{-1}}$ ($x > 2.217$ Å) as well as $E > 1.36 \times 10^9\,\mathrm{V\,m^{-1}}$ ($x < 2.154$ Å). Hence, the comparison of our predictions with experiment will be performed first for the Helmholtz layer and subsequently for hydration shells of ions. We argue that the phase (A) of H_2O compressed and with complete orientational order can represent a layer (close to a monomolecular layer) at an electrode [2], or portions of a phase dispersed in the space in the form of hydration shells of ions.

3.2 The Helmholtz Layer

The earlier publications reporting synchrotron X-ray scattering experiments on double layers at electrodes [4,5] provided results for two discrete field values only (cf. [6]), and later still one value has been deduced [17] from these data, see Fig. 13. How much water is compressed in the field? The ratio $d^{-1} = v^i/v^o$

$$d^{-1} = \frac{v^i}{v^o} = \frac{\rho^o}{\rho^i} \tag{49}$$

of specific volumes in the field and outside the field, respectively, is a function of the surface charge density σ_o.

3.2.1 *Comparison with X-ray Surface Scattering Studies*

The two triangles (Δ) in Fig. 13 correspond to H_2O densities in the first layers of molecules at the electrode [4]: one for the surface charge density $|\sigma_0| = 0.1\,\mathrm{C\,m^{-2}}$ ($E = 11.3 \times 10^9\,\mathrm{V\,m^{-1}}$), the other one for $|\sigma_0| = 0.25\,\mathrm{C\,m^{-2}}$ ($E = 28.2 \times 10^9\,\mathrm{V\,m^{-1}}$). Both belong to the compressed phase A of H_2O ($d^{-1} < 1$) with complete orientational order ($\langle \cos\theta \rangle = 1$). For $|\sigma_0| = 0.25\,\mathrm{C\,m^{-2}}$ also the second layer of H_2O molecules belongs to phase A (cf. Table I in [17]). This is represented by a diamond ($\diamond$) (at $E = 7 \times 10^9\,\mathrm{V\,m^{-1}}$) in Fig. 13. The two experimental points marked by triangles (Δ) lie only slightly out the full line ($d^{-1}(\sigma_0)$). References [4,5] showed only the presence of a dense phase, but did not indicate a phase transition yet. Phase transitions were reported "under the extremely high interfacial electric field ($\sim 10^9\,\mathrm{V/m}$)" in [2]. This very field strength value lies between the two dashed lines (shown in Fig. 13) positioned at $E = 1.36 \times 10^9\,\mathrm{V\,m^{-1}}$ and $E = 0.77 \times 10^9\,\mathrm{V\,m^{-1}}$ (see Table I for the corresponding values of σ_0), a range said above to reveal a coexistence of phase B and A.

3.2.2 *Thermal Effect at the Transition*

Yet another study concerned the mercury–aqueous electrolyte interface. By laser temperature jump method at 20°C thermal phenomena have been observed [45,50] which were interpreted by the authors as accompanying a phase transition. In a field of strength $10^9\,\mathrm{V\,m^{-1}}$, from the data and equations given in [45], we have calculated a change in entropy S of $4.2\,\mathrm{J\,mole^{-1}\,K^{-1}}$, a quantity of the same order of magnitude as that seen in Fig. 11 near Π_t – the transition value of electrostriction pressure. In our Fig. 11, a discontinuity in entropy is seen thanks to the fact that it shows the entropy as a function of electrostriction pressure Π and not the charge surface density at the electrode, as in [45]. Hence, according to our approach, one encounters here a *latent heat of a discontinuous transition*. Note that if the entropy were plotted as a function of E, its discontinuous character at the transition would not be apparent (cf. Fig. 14), since the field E itself (treated as a thermodynamic variable) also experiences a jump at the same point as the entropy.

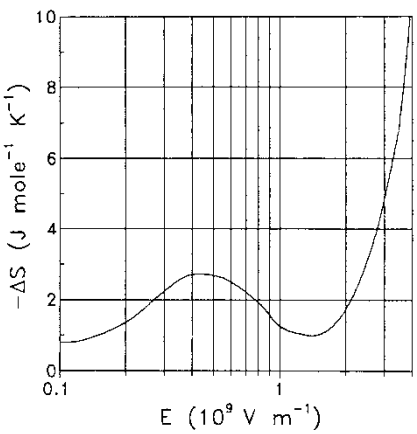

FIGURE 14 Entropy change $-\Delta S$ as a function of the electric field strength E.

3.2.3 *Comparison with Photoacoustic Studies*

As already mentioned, Kasinski *et al.* [1] demonstrated, by surface transients grating spectroscopy, the phase change to a rigid (solid) H_2O layer at the highly polar TiO_2–aqueous electrolyte interface. They estimated that "in the presence of a 1 eV liquid junction, the surface charge is of the order of $10^{14}/cm^2$". It means about one elementary charge per nm^2, or $\sim 0.16\,C\,m^{-2}$, which, according to our approach (cf. [17], Table I therein), fully corresponds to the conditions needed for obtaining (solid) layers of relative density ~ 1.8. On the other hand, Harata *et al.* [3] *assumed* a density of $1.56\,g\,cm^{-3}$ ($d^{-1} = 0.64$) to explain the results of their transient reflection grating photoacoustic experiments at gold–aqueous acidic solutions interfaces. These data to the reported accuracy agree quantitatively with the predictions made on the basis of the approach reported in this work.

3.3 Hydration Shells of Ions

Now, we shall apply our knowledge on the phases of H_2O in high electric field to interpretation of the literature data concerning the hydration shells of ions [51–53]. Along the lines of our approach, for instance, a solution can be suggested of the problem of anomalous hydration of the Sr^{2+} ion [16,54]. The steep variations (Fig. 13) of $d^{-1}(x)$ and $\langle \cos\theta \rangle$ point out that water in the vicinity of an ion is very inhomogeneous. Consequently, the first and second hydration shells show marked differences in density and permittivity. We argue that our approach draws a picture consistent with what can be deduced from the neutron diffraction isotopic substitution experiments [55,56]. The first shells of the ion Li^+, and cations doubly (maybe with a few exceptions: Ca^{2+}, Hg^{2+}, Sr^{2+}), triply and more times charged with the elementary charge reside in phase A, since the reduced radii of the first hydration shells of these cations fulfill the inequality $x_1 < 2.154\,Å$. The second shell with $x_2 > 2.217\,Å$ has been observed about most of them. The values of water density in the first shells of many ions were calculated in [7] and are given in Tables III–VI, whereas Table II contains our newly calculated data for quadruply charged ions. In literature one encounters coordination numbers h_1 [51,52,57]. The latter can be obtained from our density data with the help of the volumes of hydration shells given by Hahn [58]. From Fig. 4(a) therein the values of the volume of the first hydration sphere (in cm^3 per mole) of the ions (as a function of the ion radius R_c) have been read out and expressed as v_1 (in $Å^3$ per cation). The volumes v_1 given in Tables III–VI follow from the parabolic fits to the data given in [58] (cf. also [7]). The volumes v_1 of tetravalent cations (Table II)

TABLE II Properties of the first hydration shells of ions – case of quadruply charged cations. x_1 – reduced radius (in Å) after [51,52,55], ϵ_1 – permittivity (Eq. (22)), v_1 – volume (in $Å^3$ after [7,58], see text), ρ_1 – mass density (in $g\,cm^{-3}$), Π – local electrotriction pressure (in GPa), h_1^c – coordination number (calculated applying our method in [7]), h_1^r – coordination number (taken from literature), X, ND – X-ray and neutron diffraction, respectively, MD – molecular dynamics, MC – Monte Carlo

Ion	x_1	ϵ_1	v_1	ρ_1	Π	h_1^c	h_1^r	*Method*	*Ref.*
Pu^{4+}	1.195	2.46	80.7	2.37	32	6.4			[68]
Np^{4+}	1.2	2.47	82.15	2.32	29	6.3			[68]
U^{4+}	1.25	2.58	83.6	2.19	2	6	7.9–9.2	X	[53]
Th^{4+}	1.26	2.62	87.3	2.17	22	6.3	5–8.1	X	[53]

TABLE III Same as Table II for triply charged cations

Ion	x_1	ϵ_1	v_1	ρ_1	Π	h_1^c	h_1^r	*Method*	*Ref.*
Al^{3+}	1.10	2.34	83	2.7	49	7.4	6	X	[51,52,55]
Ga^{3+}	1.13	2.39	86	2.6	42	7.4	6	X	[69]
Cr^{3+}	1.15	2.41	90	2.4	38	7.35	6	X	[51,52,55,69]
								ND	[70,71]
Fe^{3+}	1.17	2.44	94	2.4	34	7.45	6	X	[51,52]
								ND	[72]
Rh^{3+}	1.18	2.46	95	2.4	33	7.4	6–6.3	X	[52,55,69,73]
In^{3+}	1.25	2.58	110	2.2	23	7.9	6	X	[55]
Tl^{3+}	1.29	2.67	120	2.1	19	8.4	6	X	[55]

TABLE IV Same as Table II for triply charged rare earth ions

Ion	x_1	ϵ_1	v_1	ρ_1	Π	h_1^c	h_1^r	*Method*	*Ref.*
Yb^{3+}	1.34	2.77	130	2.05	15	8.9	7.8	ND	[55]
Lu^{3+}	1.35	2.79	135	2	15	9.2	7.3–8	X	[58,52,55]
Tm^{3+}	1.36	2.81	140	2	14	9.4	7.3–8.1	X	[52,55]
Er^{3+}	1.37	2.83	140	2	13	9.5	7.8–8.2	X	[58,55]
Dy^{3+}	1.38	2.87	145	2	13	9.5	7.9–8.1	X	[58,55]
							7.4–8	ND	[55]
Tb^{3+}	1.39	2.89	150	1.95	12	9.7	7.5–8.2	X	[58,55]
Gd^{3+}	1.39	2.89	150	1.9	12	9.7	7.6–9.9	X	[52,55]
Eu^{3+}	1.41	2.94	150	1.9	11	9.6	8.3–8.6	X	[74,55]
Sm^{3+}	1.43	2.99	160	1.85	10	10	8.8–9.9	X	[74,52,55]
Nd^{3+}	1.45	3.05	165	1.85	9.5	10	8.9–9.5	X	[75,55]
							8.5	ND	[55]
Pr^{3+}	1.47	3.12	170	1.85	8.8	10.5	9.2–9	X	[75,55]
La^{3+}	1.49	3.19	180	1.8	8	10.9	9–9.1	X	[75,55]

TABLE V Same as Table II for doubly charged ions

Ion	x_1	ϵ_1	v_1	ρ_1	Π	h_1^c	h_1^r	*Method*	*Ref.*
Be^{2+}	1.18	2.46	80	2.4	32.5	6.4	4	X	[55]
Cu^{2+}	1.40	2.91	110	1.9	12	6.9	4	X	[51,55]
							3.4–4.1	ND	[76]
Ni^{2+}	1.46	3.08	120	1.85	9	7.2	6	X	[51,55]
							5.4–8	ND	[52,77]
Co^{2+}	1.48	3.16	120	1.8	8	7.3	5–6.3	X	[52]
Mg^{2+}	1.50	3.22	120	1.8	8	7.4	6–8	X	[52]
							6	MD	[52]
Fe^{2+}	1.50	3.22	120	1.8	8	7.4	5.1–6	X	[52]
							6	ND	[72]
Zn^{2+}	1.51	3.25	125	1.8	7.2	7.4	6	X	[51,52]
Mn^{2+}	1.55	3.41	130	1.75	6	7.7	6	X	[55]
							5	ND	[55]
Sn^{2+}	1.56	3.44	130	1.7	5.9	7.7	2.4–3.8	X	[52]
Cd^{2+}	1.62	3.72	140	1.7	4.5	8	6.9–8.8	X	[52]
Ca^{2+}	1.70	4.19	160	1.35	3.2	7.1	6–8	X	[52]
							6.4–10	ND	[55,78]
							9.2	MD	[52]
Hg^{2+}	1.70	4.19	160	1.35	3.2	7.1	6	X	[52,55]
Sr^{2+}	1.87	5.83	190	1.2	1.4	8.5	8, 7.3	X	[51,79]
Sr^{2+}	~ 2.2	34.25					15 ± 1	ND	[54]

TABLE VI Same as Table II for singly charged cations

Ion	x_I	ϵ_I	v_I	ρ_I	Π	h_1^c	h_1^r	*Method*	*Ref.*
Li^+	1.95	7.29	110	1.2	0.75	4.4	4	X	[55]
							5.5–6	ND	[55,80]
							6	MD	[52,80]
							4–5.3	MC	[80]
Na^+	2.40	56.7	160	1.0	$\sim 10^{-4}$	5.3	5–6	X	[55]
							4.9–6	ND	[55,80]
							6–7	MD	[52]
							4.3–6	MC	[80]
Ag^+	2.40	56.7	160	1.0	$\sim 10^{-4}$	5.3	2–4	X	[52]
							3.7–4.1	ND	[55,80]
K^+	2.70	68.6	180	1.0	$\sim 10^{-4}$	6.1	6; 4	X	[52,55]
							3.9–8	ND	[80, 52]
							6.6–7.6	MD	[52,80]
							5.1–7.5	MC	[80]
Rb^+	2.89	72.8	190	1.0	$\sim 10^{-4}$	6.5	5.6	X	[81,82]
Cs^+	3.15	75.6	205	1.0	$\sim 10^{-4}$	6.8	3–8	X	[52,55]
							7–7.9	MD	[52]
Tl^+	3.20	76.1	205	1.0	$\sim 10^{-4}$	6.9	4	X	[55]

have been calculated according to Eq. (21) in [58] on applying the Pauling radii. The coordination numbers h_1 have been calculated according to the formula:

$$h_1 = \frac{\rho_1 v_1}{M}, \tag{50}$$

where M is the mass of a water molecule. Our calculated values of the coordination numbers h_1 are compared with those in literature (Tables II–VI). The reduced radii of the second shells of these cations are such that the water at these distances belongs to phase B. The properties of their second shells are shown in Fig. 13: $d^{-1} = 1$, as in the bulk water with no applied field, and $\langle \cos\theta \rangle < 0.98$ ($\epsilon > 38$). The first shells of monovalent cations, except Li^+, and the first shells of anions: F^-, Cl^-, Br^-, and I^- (formed at reduced distances $x > 2.217$ Å, cf. [12], Table II therein) belong also to phase B. Water in their shells is not compressed. On the basis of the thermodynamic calculations only one cannot judge whether H_2O in phase A compressed by the field is fluid or solid. Although the complete directional ordering of the dipoles is known, one does not know which space structure they form. A theoretical hint could follow a possible calculation of the stiffness of this phase, and the experimental evidence collected so far [1,2] speaks in favor of a solid.

3.3.1 Comparison with the Neutron Scattering Studies

Figure 15 presents the isotherm $\Pi(x)$ at 298 K as a function of the reduced distance x from the center of an ion. In the plot of $\Pi = \Pi(x)$ in Fig. 15, the discontinuity in the electric field strength is extended over the range $2.154 < x < 2.217$ Å. The plots of the relations $\Pi = \Pi(x)$ are steeper for $x < 2.154$ Å than for $x > 2.217$ Å. For $x > 2.217$ Å one finds phase B whereas for $x < 2.154$ Å one encounters phase A. In addition to the x discontinuity, the change in the slope of the isotherm plotted in Fig. 15 is interpreted as testifying to a phase transition: phase A $\rightarrow$ phase B under the electrostriction pressure $\Pi_t = 0.21$ GPa. It will be argued that the discontinuity of

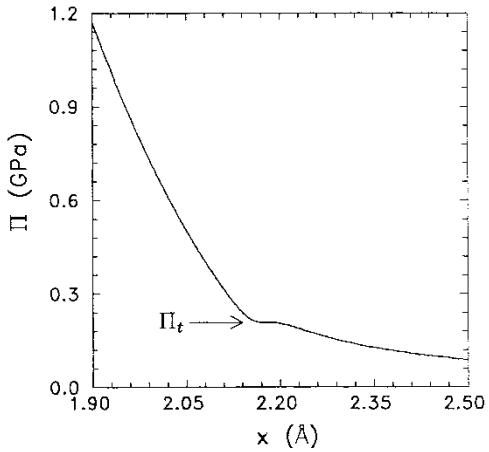

FIGURE 15 Electrostriction pressure $\Pi(x)$ as a function of the reduced distance x from the centre of the ion. The arrow marks the transition value Π_t of the electrostriction pressure.

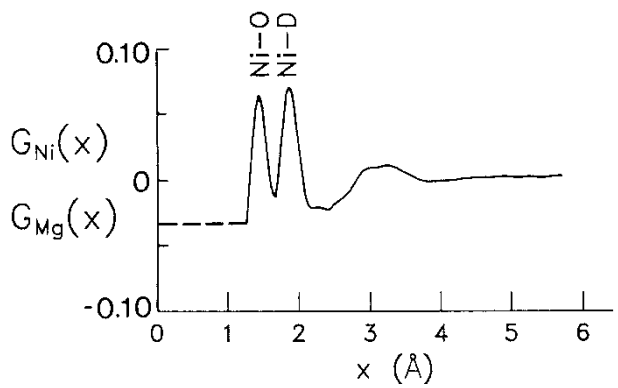

FIGURE 16 Total cation (Ni^{2+}, Mg^{2+}) distribution functions $G_{Ni}(x)$ and $G_{Mg}(x)$ (in units barn sr^{-1}); after [59]. Ni^{2+} is isomorphic with Mg^{2+} in D_2O solution.

the transition which allows for a whole range of x to correspond to the transition value Π_t of the electrostriction pressure explains the destroyed hydration structure phenomenon of Sr^{2+} ion ([59] and references cited therein). The calculated properties of the phases A and B are in our opinion also consistent with the known results of neutron scattering studies of other ions in D_2O solution. Marcus [52] has indicated the following additivity relation between the distance ion-water (r_1, equal to the radius of the first hydration shell) and the ionic radius R_c, as well as the radius of a water molecule ($R_{water} \approx 1.4$ Å): $r_1 = R_c + R_{water}$. Hence, the corresponding reduced distance

$$x_1 = (R_c + R_{water})/\sqrt{Z}. \tag{51}$$

3.3.1.1 First Hydration Shells of Ions in Neutron Scattering Studies Figure 16 shows the total RDF's $G_{Ni}(x)$ and $G_{Mg}(x)$ (Ni^{2+} is isomorphic with Mg^{2+} in aqueous solution) typical of cations with the reduced radii x_1 of the first hydration shells $x_1 < 2.154$ Å. The

first of the two sharp peaks in the plot of $G_{Ni}(x)$ is attributed to the distance Ni–O (cation-oxygen of heavy water molecule), the other one – to Ni–D. Such a shape of the function $G_{cation}(x)$ follows the well-defined hydration structures in solution. The additivity relation (Eq. (51)) holds for such ions. Ni^{2+} and Mg^{2+} form fairly well-defined long-lived [59] hydration structure in solutions. This characteristics of the well-defined hydration structures [59] (first hydration shell), learned from the experimental RDF's, is consistent with the characteristics of phase A. The calculated densities of the hydration shells can be expressed in terms of the coordination numbers of specific ions which are given in Tables II–VI and are compared with literature data. We conclude that the concept of the phase A of water, dense and orientationally ordered in a field, is not in conflict with the known data.

3.3.1.2 Behavior of a Hydration Shell at the Phase Transition: Destroyed Hydration Structure of the Sr^{2+} Ion The lack of resolved two peak structure in the RDF of hydration shells of ions together with the accompanying lack of additivity of the ion and H_2O radii (violation of Eq. (51)) has been found in the shell of Ni^{2+} ion at 573 K and called the *destroyed hydration structure* [37,60]. An RDF showing the destroyed hydration structure characteristics had been obtained earlier in [54] by the neutron scattering method for the Sr^{2+} ions at ambient conditions (see Fig. 17), although at the time the term "destroyed hydration structure" was not coined yet. The radial distribution function $G_{Sr}(x)$ about the Sr^{2+} ions is characterized by a single broad peak centered at $x = 2.23$ Å. This value does not fulfill Eq. (51), which indicates a lack of additivity of ionic and molecular radii. The discontinuity in x ($2.154 < x < 2.217$ (Å)) at Π_t falls entirely within a broader range of x values under the single broad peak of the neutron scattering RDF $G_{Sr}(x)$ (Fig. 17). Let us recall that in our description the state of H_2O in the hydration shell is defined by the state variables T, Π, x. To each value of Π on the 298 K isotherm $\Pi(x)$ in Fig. 15 there corresponds a given x value except for Π_t, at which x takes any value from the range $2.154 < x < 2.217$ (Å). We proposed [16] an interpretation of the apparently hitherto unexplained peculiar character of the neutron scattering RDF called the destroyed hydration structure: RDF smearing and lack of additivity of ionic and water radii. According to this interpretation, it can be a consequence of a discontinuity in x at the phase transition point. In such a case water in the neighborhood of the ion is in

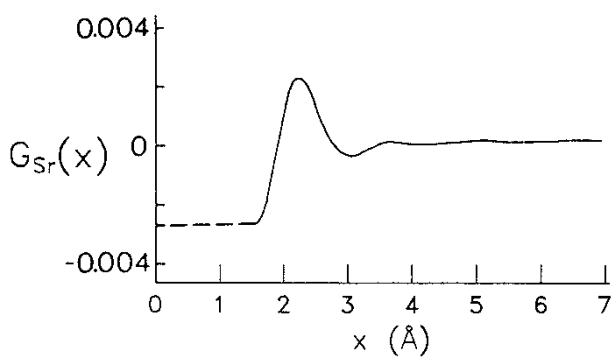

FIGURE 17 Total cation (Sr^{2+}) distribution function $G_{Sr}(x)$ (in units barn sr^{-1}); after [59].

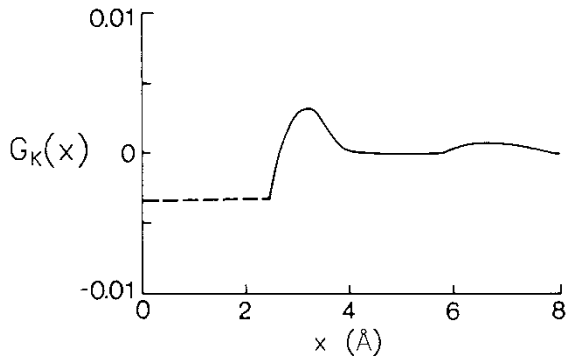

FIGURE 18 Total cation (K^+) distribution function $G_K(x)$ (in units barn sr^{-1}): after [59].

the state determined by Π_t and a water molecule can choose any possible value of the reduced radius x from the above mentioned range (Fig. 15). Hence, there is no specific unique value of x_t corresponding to Π_t, but any x value in the range is acceptable. H_2O molecules in this state can statistically take positions at different distances from the ion. This statistical freedom of taking different distances results in the effect called the destroyed hydration structure: the peaks in RDF attributed to oxygen and deuterium are broadened and shifted so as to give a common broad peak with a maximum not fulfilling the criterion given by Eq. (51).

3.3.1.3 Shells of Weakly Hydrated Ions in Neutron Scattering Studies The comparable data for K^+ are shown in Fig. 18. The reduced radius of its first hydration shell is $x_1 > 2.217$ Å. The RDF $G_K(x)$ is characterized by a single maximum [59], whose position is close to the reduced distance $x_1 = 2.8$ Å, obtained from Eq. (51). From Table XIII in [52], it follows that other ions bearing single elementary charges (for which $x_1 > 2.217$ Å) fulfill Eq. (51) also. The absence of two clearly resolved peaks in $G_K(x)$ is a clear evidence that K^+ is weakly hydrated. This characteristics of weakly hydrated ions [59] read from $G_K(x)$ is consistent with the characteristics of phase B following from our approach: $\langle \cos\theta \rangle < 1$, $\epsilon > 38$ (which means a lack of a full orientational order), and no remarkable compression: $d \to 1$. Again, the concept of phase B – a weakly ordered liquid water phase – is not in conflict with the previous knowledge.

3.3.2 The Dynamic Hydration of Ions

The hydration of ions is in general described by the number h_1 of water molecules in the first hydration shells and their number h_2 in the second hydration shells. The sum:

$$h = h_1 + h_2 \tag{52}$$

is called the dynamic hydration number [61]. Volumes v_1 and v_2 per water molecule in the first and second hydration shells, respectively, *vs* crystallographic radius R_c for trivalent lanthanide ions have been investigated by David and Fourest [61] through transport properties using radiochemical methods. From the R_c, h_1, h_2, v_1, and v_2

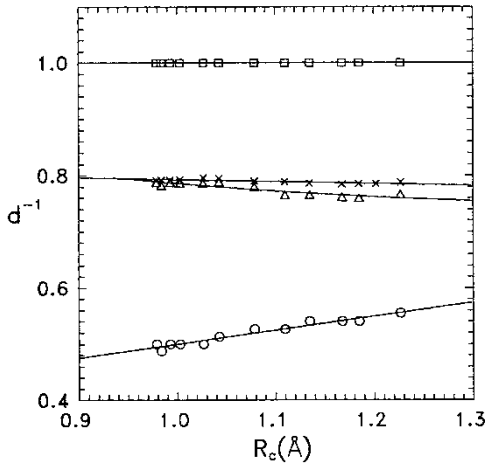

FIGURE 19 Variaiton of the relative volume $d^{-1}$of H_2O in the primary ○ $(d^{-1})_1$ and secondary □ $(d^{-1})_2$ hydration shells *vs* crystallographic radius R_c for trivalent lanthanide ions. Plot of the quantity $\langle d^{-1}\rangle_h$ has been given (line with data marked Δ). The latter line presents the data calculated with the help of Eq. (53), with the quantities $(d^{-1})_1$ ○ and $(d^{-1})_2$ □ obtained with the method presented in this work. For the sake of comparison, yet another quantity $\langle d^{-1}\rangle_h$ calculated with the help of Eq. (53) but from the data obtained by David and Fourest [61] is shown (line with data marked ×).

data of [61] Tables I and II therein) we calculate the mean value $\langle d^{-1}\rangle_h$ – mean specific volume per water molecule in both the first and second hydration shells:

$$\langle d^{-1}\rangle_h = \frac{h_1(d^{-1})_1 + h_2(d^{-1})_2}{h_1 + h_2} \tag{53}$$

where

$$(d^{-1})_1 = \frac{v_1}{v_o} \quad \text{and} \quad (d^{-1})_2 = \frac{v_2}{v_o}. \tag{54}$$

The volume per water molecule in the bulk is $v_o = 30\,\text{Å}^3$. The quantity $\langle d^{-1}\rangle_h$ calculated with the help of Eq. (53) from the data obtained by David and Fourest [61]) is shown in Fig. 19 (line marked ×). For the sake of comparison, yet another plot of the quantity $\langle d^{-1}\rangle_h$ has been given therein (line marked Δ). The latter line presents the data calculated also with the help of Eq. (53), but with the quantities $(d^{-1})_1$ and $(d^{-1})_2$ obtained according to the method presented in this work (with v_1 given in Table II and $v_2 = v_o$). Our calculated values of $(d^{-1})_1$ (line marked ○) are lower, and our calculated values of $(d^{-1})_2$ (line marked □) are higher than the corresponding data by David and Fourest [61] (not shown). Nevertheless, the relative difference between the $\langle d^{-1}\rangle_h$ values obtained with these two completely different methods (that of [61] × and the present one Δ) is small and amounts to about 2%. The authors of [61] have written that their "calculations have been adjusted...to fit the experimental data" [61]. Let us remind once again that our approach contains *no* adjustable parameters. Anyway, from the numerical agreement between the results of the aforementioned theoretical calculations (this work) on the one hand, and the experimental [61] data on the other hand, we draw the conclusion that our method leads to correct values of H_2O density in the dynamical hydration shells of lanthanides.

3.4 Protein Hydration in Solution

Characterization of the physical properties of protein surface hydration water is a subject of current interest (cf. [8,62] and references therein). Three proteins: chicken egg white lysozyme, thioredoxine reductase from *Escherichia coli*, and ribonucleotide reductase protein R1 of *E. coli*, were investigated by Svergun *et al.* [8] in parallel by X-ray and neutron scattering in H_2O and D_2O solutions. They noted that "the scattering density in the border layer was typically 1.05–1.25 times that of the bulk, suggesting that the hydration shell around proteins is denser than the bulk solvent". Within the framework of the theory presented in this work, we are able to relate the density of water of the hydration shells around proteins with the electric field on the surface of the protein. The authors of [62] have found that the strength of the field is correlated with the H_2O density over the most highly populated field values, with higher field strength accompanying higher density. These highly populated field values given in [62] are related to the surface charge density σ values ($0.005–0.03\, q\, \text{Å}^{-2}$), representing the source of the electric displacement vector ϵE, and are useful for comparison of the results obtained by means of our approach with these by Svergun *et al.* [8]. In Figs. 20 and 21 is plotted the relation $d = d(\sigma)$, following from the equation:

$$\frac{V}{\epsilon_o}\left\{\frac{\partial}{\partial \epsilon}\int_0^y \frac{\sigma}{\epsilon} d\left[\sigma\left(1-\frac{1}{\epsilon}\right)\right]\right\}\left(\frac{\partial \epsilon}{\partial N}\right)_{T,V,\sigma} = \int_{1\text{atm}}^{P^i} \frac{\partial V}{\partial N}\, dP \tag{55}$$

being another form of Eq. (43) with each value of the quantity d read from the empirical isotherm [46–48] for the corresponding value of P^i; σ is a state parameter in this equation of state. Since in [8] $1.05 < d < 1.25$, our values of σ: $0.282 < \sigma < 0.351$ (C m^{-2})

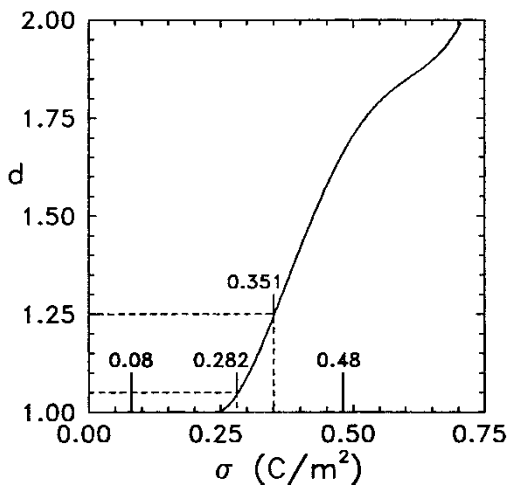

FIGURE 20 The relative mass density $d(\sigma)$ values as a function of the surface charge density σ. On the abscissa there are marked the values of σ corresponding to the limits of the "highly populated field values" in the hydration layer of a protein molecule [62]: 0.08 and $0.48\,\text{C m}^{-2}$ and on the ordinates – the limits of the values of d, 1.05–1.25, found in [8]. The values of the abscissa $0.282 < \sigma < 0.351$ (C m^{-2}) calculated with the help of this curve (cf. Table VII) fall within the range $0.08 < \sigma < 0.48$ (C m^{-2}) corresponding to those "highly populated field values" [62].

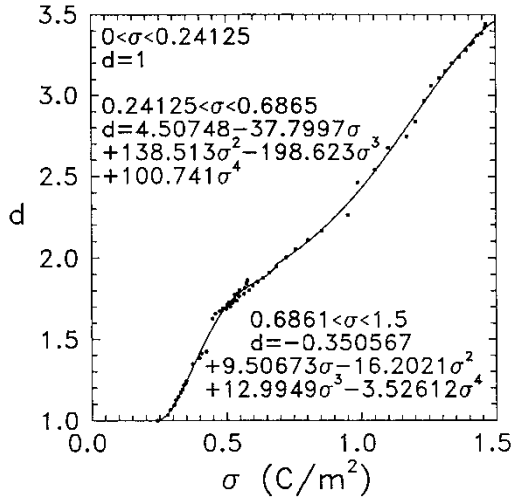

FIGURE 21 Points marking the relative mass density $d(\sigma)$ values as a function of the surface charge density σ. Three fitting polynomials in three separate ranges of the independent variable σ are written. $d = 1$ in the range $0 \le \sigma \le 0.24125$ ($C\,m^{-2}$). A fitting polynomial of the 4th order in σ belongs to the range $0.24125 \le \sigma \le 0.6865$ ($C\,m^{-2}$) and yet another one – to the range $0.6861 \le \sigma \le 1.5$ ($C\,m^{-2}$).

TABLE VII Permittivity ϵ, relative density d and surface charge density σ for several values of electric field E at the surface of the proteins

σ [$q/Å^2$]	0.005 [62]	0.018	0.022	0.03 [62]
σ [C/m^2]	0.08	0.282	0.351	0.48
E [10^9 V/m]	0.11	1.82	6.20	14.86
ϵ	80.1	17.48	6.4	3.75
d	1	1.05 [8]	1.25 [8]	1.685

(cf. Table VII and Fig. 20), calculated on the basis of these data (e.g., with the help of Fig. 22), are situated within the range $0.08 < \sigma < 0.48\,C\,m^{-2}$ corresponding to those "highly populated field values" given in [62]. Hence, the values of the electric field E calculated in this work on the basis of the values of the density of water in the hydration shell around proteins found in [8] are reasonable.

In Eq. (55) there appears only the square of the σ value (σ^2) (or, equivalently, the square of the *value* of the electric field strength E^2). These values are *scalar quantities*. Hence, our results are completely insensitive to the direction of the field.

Table VII presents some literature data as well as several physical quantities found by means of our phenomenological theory for selected values of E (or, equivalently, σ). The authors of [62] (cf. p. 5381 therein) have raised a question: which aspects of the protein surface determine the water density variations. Their calculations showed no clear relationship between the hydration shell water density and the chemical characteristics of the surface atoms or residues, for instance, hydrophobic/hydrophilic. However, groups with net charges, have the density increased in their neighborhood. The results collected in Table VII seem to suggest the possibility that in explaining the dense hydration shells of protein molecules on the basis of the condition of thermodynamic equilibrium the presence of electrostatic interactions plays an essential role.

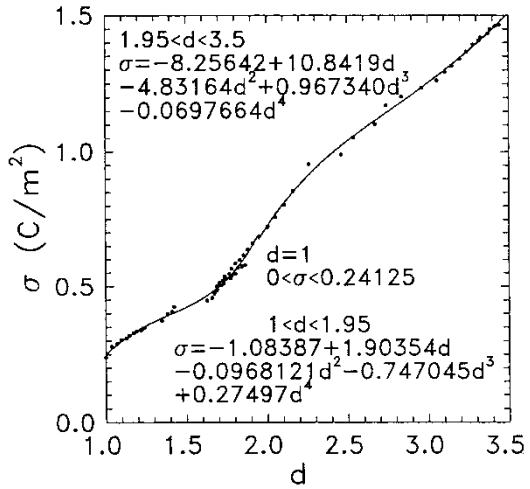

FIGURE 22 Points marking the values of the surface charge density $\sigma(d)$ as a function of the relative mass density d. For $d=1$, σ takes the values in the range $0 \leq \sigma \leq 0.24125$ ($\mathrm{C\,m^{-2}}$). For $1 \leq d \leq 1.95$ a fitting polynomial of the 4th order in d is written. For $1.95 \leq d \leq 3.50$ yet another polynomial of the 4th order in d has been fitted to the $\sigma(d)$ relation.

4. REMARKS ON THE METHOD

We shall discuss the statistical calculation of average quantities as applied to the case of water layers at charged electrodes, hydrated ions and large protein molecules. Strong electric fields generated by the charges of the ions decay rapidly with the radial distance into water according to the Coulomb law. As a consequence, the molecules within the first hydration shells are in the fields of a considerably higher strength than those outside them. In this way the first hydration shells about the ions are distinguished in respect to the field from the whole electrolyte. Taken together, the first shells form a subsystem of molecules in the same physical conditions, although they do not have a common macroscopic boundary. The chemical potentials of various parts of the system in equilibrium, including the set of the first hydration shells, the sets of the further more or less well defined shells, and the rest in zero field, are equal. The subsystem of the first shells of ions of one kind forms a macroscopically large ensemble of molecules in the same physical conditions and thus can be subjected to the procedure of statistical averaging leading to values of their thermodynamic parameters. Although dispersed in space, the set of the hydration shells can be treated in much the same way as a layer of molecular thickness in the theory of electrolytes at an electrode discussed in the current work and in [6,63]. Thus, one can derive thermodynamic quantities concerning the dispersed in space, but otherwise macroscopic, set of hydration shells of ions by statistical methods, as done throughout this paper. Another point is the applicability of the Onsager field approximation, frequently conceived after popular textbooks as forming a part of the continuum theory [64], to discrete microscopic systems such as those considered here. Note in this context that this approximation in the statistical calculations appears in the literature of atomically discrete dielectric and magnetic systems, to mention only [24–26]. Let us still mention that the electric field strength E occurring in the current work represents a thermodynamic variable

stemming from the statistical mechanics calculations based on our model assumptions in the Onsager approximation.

5. SOME PERSPECTIVES

According to Harata *et al*. [65] picosecond ultrasonics based on transient grating measurement can be applied in investigation of double layers at electrodes and ''molecules at an electrode are expected to form a highly ordered layer that is stiffer than the bulk''. This opens, in addition to the mainly structural findings of new phases by Chu *et al*. [2] by X-ray scattering, new possibilities of investigation of their mechanical, thermal and optical properties, both experimental and theoretical. Methods similar to those reviewed and applied in this paper might find applications to some problems encountered in treating biological membranes [66], where one also has to do with strong electric fields of strengths comparable to those acting on water in conditions considered here.

6. CONCLUSION

We have presented a *theoretical evidence* of a phase transition in H_2O at ambient conditions in a local field of strength taking the values in the range $0.77 < E < 1.36$ ($10^9\,V\,m^{-1}$). The *experimental evidence* of phase transitions in H_2O in a high electric field has been provided by Chu *et al*. [2]. The above E values fall well into the range in which they observed the transitions at the RuO_2 highly polar surface by synchrotron radiation X-ray scattering methods. Also, these values fall very close to the field acting on the water molecules lying at the maximum of RDF in the hydration shell of the Sr^{2+} ion, which enabled us to provide a tentative explanation of its peculiar properties revealed by neutron scattering [54]. The synchrotron X-ray experiments [2] were most essential in revealing the phase transition of H_2O in high electric field. They are corroborated by other measurements of physical quantities related to the transition to a dense phase in the field: high density [4], high mechanical stiffness deduced from sound velocity [1], and thermal effects related to the transition [45,50]. One should add the recently discussed dense hydration shells in the vicinity of protein molecules in water solutions showing local densities markedly exceeding that of the bulk water [8] and attributed to the same electrostriction effects [67]. All these very different experiments are quantitatively accounted for by the theoretical approach reported here.

The fact that such a relatively simple approach applied here leads to a number of phenomena at quantitatively correctly predicted physical conditions may be attributed, in our opinion, to two main ingredients. Firstly, the dielectric behavior (permittivity) of water, thought as a hydrogen-bonded substance, is correctly accounted for by applying a simple statistical model, which previously proved its usefulness in describing hydrogen-bonded liquids [12]. Secondly, the striction properties of water are treated realistically by using the compressibility isotherms for H_2O under high pressure (10^5 Pa to about 100 GPa) in no field [46–48], together with an *ad hoc* hypothesis (checked *a posteriori* to be true with a very good accuracy [6]), saying that they are only negligibly affected by the field. The immediate application of the latter experimental data at the level of thermodynamic relations permits avoidance of the use of adjustable parameters.

NOMENCLATURE

A = quantity defined by Eq. (21)
A = compressed phase of H_2O with complete orientational order induced by the field
B = quantity defined by Eq. (16)
B = phase of H_2O with no remarkable compression and with incomplete orientational order induced by the field
$b(I)$ = coefficient at the first term of the power series expansion of the function defined in Eq. (11)
$B_I(\Xi)$ = function defined in Eq. (11)
$c(I)$ = coefficient at the second term of the power series expansion of the function defined in Eq. (11)
$\langle \cos\theta \rangle$ = the mean cosine of the angle θ between the direction of the dipole moment μ of the water molecule and the direction of the electric field E
d = the relative H_2O density
d^{-1} = the relative H_2O volume
$D = \epsilon E$ = electric displacement
$\langle d^{-1} \rangle_h$ = mean specific volume of the water molecule in the first and second hydration sphere
E_{on} = the Onsager local field
E = the external electric field strength
$g = (\epsilon + n^2/2)$
$G(x)$ = the radial distribution function (RDF)
$h = h_1 + h_2$ = the dynamic hydration number
h_1 (h_2) = number of water molecules in the first (second) hydration shell
i = superscript marking the quantities inside the electric field
I = number of admitted orientations of the dipole moment
L = the work related to water compression in the field – the electrostriction work
$L(\Xi)$ = Langevin function
$M = 3 \times 10^{-26}$ kg – the mass of the water molecule
N^o = the Avogadro number
N/V = number density
N = number of molecules in the volume V
n = refraction index
o = superscript marking the quantities outside the electric field
P = pressure
q = elementary charge (16×10^{-20} C)
r = distance from the center of the ion
R = molar gas constant
R_c = crystallographic radius of an ion
R_{water} = radius of the water molecule
RDF = radial distribution function

RT = thermal energy (~ 2.5 kJ/mole at T ~ 300 K)
T = absolute temperature
W = work performed by the field E by reorienting the water dipoles
W_{HB} = hydrogen bond energy
$v^o = V/N^o$
V = volume of the system, taken as equal to the molar volume of water at ambient conditions
$V = V(P)$ = isotherms of H_2O
v_1 and v_2 = the volumes per water molecule in the primary and secondary hydration spheres, respectively
Vdy = the increment of the polarization of the subsystem "i"
x = reduced radius $x = r \times |Z|^{-1/2}$
x_1 and x_2 = the reduced radii of the primary and secondary hydration spheres, respectively
Z = number of excess elementary charges of an ion (valence)
α_p = thermal expansion coefficient
γ = quantity defined by Eq. (29)
ΔQ = electrocaloric effect
ϵ = permittivity
ζ = chemical potential
ζ^i = chemical potential inside the electric field
ζ^o = chemical potential outside the electric field
ζ_L = chemical potential increment related to work L done to compress water in the field
ζ_W = chemical potential increment related to work W needed to put a molecule from outside the field into the field
θ = angle between the direction of dipole moment μ and the direction of the electric field E
μ = dipole moment of the water molecule $\mu = 6.03 \times 10^{-30}$ Cm
Ξ = quantity defined by Eq. (5)
Π = local electrostriction pressure
$\Pi_t = 0.2$ GPa – transition value of the local electrostriction pressure
ρ = local density of water
σ_0 = free charge surface density
σ = total charge surface density
Ω = grand potential omega

References

[1] J.J. Kasinski, L.A. Gomez-Jahn, K.J. Faran, S.M. Gracewski and R.J. Dwayne Miller (1989). *J. Chem. Phys.*, **90**, 1253.
[2] Y.S. Chu, T.E. Lister, W.G. Cullen, H. You and Z. Nagy (2001). *Phys. Rev. Lett.*, **86**, 3364.
[3] A. Harata, Qing Shen and T. Sawada (1996). *Physica B*, **219 and 220**, 629.
[4] M.F. Toney, J.N. Howard, J. Richer, G.L. Borges, J.G. Gordon, O.R. Melroy, D.G. Wiesler, D. Yee and L.B. Sorensen (1994). *Nature*, **368**, 444.
[5] M.F. Toney, J.N. Howard, J. Richer, G.L. Borges, J.G. Gordon, O.R. Melroy, D.G. Wiesler, D. Yee and L.B. Sorensen (1995). *Surf. Sci.*, **335**, 326.

[6] I. Danielewicz-Ferchmin and A.R. Ferchmin (1996). *J. Phys. Chem.*, **100**, 17281.
[7] I. Danielewicz-Ferchmin and A.R. Ferchmin (1998). *Physica.*, **B 245**, 34.
[8] D.I. Svergun, S. Richard, M.H.J. Koch, Z. Sayers, S. Kuprin and G. Zaccai (1998). *Proc. Natl. Acad. Sci. USA*, **95**, 2267.
[9] A. Brodsky (1996). *Chem. Phys. Lett.*, **261**, 563.
[10] H.S. Frank (1955). *J. Chem. Phys.*, **23**, 2023.
[11] L.D. Landau and E.M. Lifshits (1951). Statisticheskaya fizika (Izd. Tekh-Teor. Lit., Moskva, 1951), Section 25, in Russian; idem, Elektrodinamika sploshnych sred, ibid., 1957, Section 15, in Russian.
[12] I. Danielewicz-Ferchmin (1995). *J. Phys. Chem.*, **99**, 5658.
[13] N.H. March (1990). *Chemical Physics of Liquids*. Gordon and Breach, London.
[14] J.B. Hasted (1972). *Dielectric and Related Molecular Processes*, *Senior Reporter Mansel Davies*. The Chemical Society, Burlington House, London.
[15] I. Danielewicz-Ferchmin and A.R. Ferchmin (2002). *J. Solution Chem.*, **31**, 81.
[16] I. Danielewicz-Ferchmin and A.R. Ferchmin (2003). *Phys. Chem. Chem. Phys.*, **5**, 165.
[17] I. Danielewicz-Ferchmin, A.R. Ferchmin and A. Szlaferck (1998). *Chem. Phys. Lett.*, **288**, 197.
[18] H. Frölich (1958). *Theory of Dielectrics*, 2nd Edn. Oxford University Press, Oxford.
[19] C.J.F. Böttcher, O.C. van Belle, P. Bordevijk and A. Rip (1973). *Theory of Electric Polarization*, 2nd Revised Edn., Vol. 1. Elsevier, Amsterdam.
[20] C. Kittel (1966). *Introduction to Solid State Physics*, Chapter 14. Wiley, New York.
[21] J.S. Smart (1966). *Effective Field Theories of Magnetism*, Chapter 1. W. B. Saunders Company, Philadelphia.
[22] Yi Luo, H. Ågren, and K.V. Mikkelsen (1997). *Chem. Phys. Lett.*, **275**, 145.
[23] L. Sandberg and O. Edholm (2002). *J. Chem. Phys.*, **116**, 2936.
[24] T. Kaneyoshi (1969). *Prog. Theor. Phys.*, **41**, 577.
[25] T. Kaneyoshi (1971). *Prog. Theor. Phys.*, **45**, 1340.
[26] D.E. Logan, Y.H. Szczech and M.A. Tusch (1995). *Europhys. Lett.*, **30**, 307.
[27] H. Eyring and M.S. Jhon (1969). *Significant Liquid Structures*. Wiley, New York.
[28] L. Pauling (1935). *J. Am. Chem. Soc.*, **57**, 2680.
[29] R.H. Cole (1989). *Annu. Rev. Phys. Chem.*, **40**, 1.
[30] I. Danielewicz-Ferchmin (1990). *Indian J. Pure Appl. Phys.*, **28**, 512.
[31] P.A. Bradley, G. Parry Jones, H.A. Kolodziej and M. Davies (1975). *J. Chem. Soc. Faraday Trans II* (*GB*), **71**, 1200.
[32] A.E. Davies, M.J. van der Sluijs, G. Parry Jones, and M. Davies (1978). *J. Chem. Soc. Faraday Trans. II* (*GB*), **74**, 571.
[33] I. Danielewicz-Ferchmin and A.R. Ferchmin (1998). *J. Chem. Phys.*, **109**, 2394.
[34] D.C. Grahame (1953). *J. Chem. Phys.*, **21**, 1054.
[35] J. Padova (1963). *J. Chem. Phys.*, **39**, 1552 (Fig. 1).
[36] E. Glueckauf (1964). *Trans. Faraday Soc.*, **60**, 1637.
[37] I. Howell, and G.W. Neilson (1996). *J. Chem. Phys.*, **104**, 2036.
[38] I. Danielewicz-Ferchmin (1972). *Acta Phys. Polon.*, **A42**, 699.
[39] D. Eisenberg and W. Kauzmann (1969). *Structure and Properties of Water*. Oxford Unviersity Press, London.
[40] M. Peschke, A.T. Blades, and P. Kebarle (1998). *J. Phys. Chem.* A., **102**, 9978.
[41] M. Pavlov, P.E.M. Siegbahn and M. Sandström (1998). *J. Phys. Chem. A*, **102**, 219.
[42] G.W. Toop (1995). *Metallurg. Mater. Trans.*, **26 B**, 577.
[43] T. Balcerzak (1998). *J. Magn. Magn. Mat.*, **177**–**181**, 771.
[44] I. Danielewicz-Ferchmin and A.R. Ferchmin (2002). *Chem. Phys. Lett.*, **351**, 397; errata ibid. (2002) **358**, 357.
[45] V.A. Benderskii, A.M. Brodsky, G.I. Velichko, L.I. Daikhin, N.S. Lidorenko and G.F. Muchnik (1986). *Dokl. Akad. Nauk SSSR*, **286**(3), 648 (in Russian).
[46] A. Polian and M. Grimsditch (1983). *Phys. Rev. B*, **27**, 6409.
[47] R.J. Hemley, A.P. Jephcoat, H.K. Mao, C.S. Zha, L.W. Finger and D.E. Cox (1987). *Nature*, **330**, 737.
[48] S.P. Clark, Jr. (Ed.) (1966). *Handbook of Physical Constants*, Revised Edn. The Geological Society of America, Inc., New York.
[49] F. Bruni, M.A. Ricci and A.K. Soper (2001). *J. Chem. Phys.*, **114**, 8056.
[50] A.M. Brodsky and L.I. Daikhin (1989). *Elektrokhim.*, **25**(4), 435 (in Russian).
[51] M. Magini, G. Licheri, G. Paschina, G. Piccaluga and G. Pinna (1988). *X-ray Diffraction of Ions in Aqueous Solutions*. CRC Press, Inc., Boca Raton, Florida.
[52] Y. Marcus (1988). *Chem. Rev.*, **88**, 1475.
[53] H. Ohtaki and T. Radnai (1993). *Chem. Rev.*, **93**, 1157.
[54] G.W. Neilson and R.D. Broadbent (1990). *Chem. Phys. Lett.*, **167**, 429.
[55] G.W. Neilson and J.E. Enderby (1989). *Adv. Inorg. Chem.*, **34**, 195.
[56] G.W. Neilson, P.E. Mason, S. Ramos and D. Sullivan (2001). *Phil. Trans. R. Soc. Lond. A*, **359**, 1575.
[57] J.E. Enderby (1995). *Chem. Soc. Rev.*, **24**, 159.

[58] R.L. Hahn (1988). *J. Phys. Chem*., **92**, 1668.
[59] I. Howell, G.W. Neilson and P. Chieux (1991). *J. Mol. Structure*, **250**, 281.
[60] P.H.K. de Jong, G.W. Neilson and M.-C. Bellisent-Funel (1996). *J. Chem. Phys*., **105**, 5155.
[61] F.H. David and B. Fourest (1997). *New J. Chem*., **21**, 167.
[62] F. Merzel and J.C. Smith (2002). *Proc. Natl. Acad. Sci. USA*, **99**, 5378.
[63] S. Romanowski, W. Stasiak and L. Wojtczak (1982). *Electrochim. Acta*, **27**, 511.
[64] In-Chul Yeh and M.L. Berkowitz (2000). *J. Chem. Phys*., **112**, 10491.
[65] A. Harata, Qing Shen and T. Sawada (1999). *Annu. Rev. Phys. Chem*., **50**, 193; see p. 214.
[66] K. [A.] Lebedev, S. Mafé, A. Alcaraz and P. Ramírez (2000). *Chem. Phys. Lett*., **326**, 87.
[67] I. Danielewicz-Ferchmin, E. Banachowicz and A.R. Ferchmin (2003). *Biophys. Chem*., **106**, 147.
[68] V. Neck and J.I. Kim (2001). *Radiochim. Acta*., **89**, 1.
[69] A. Muńoz-Páez., S. Díaz, P.J. Pérez, M.E. Martín-Zamora, J.M. Martínez, R.R. Pappalardo and E. Sánchez Marcos (1995). *Physica B*, **208 and 209**, 395.
[70] P.S. Salmon, G.J. Herdman, J. Lindgren, M.C. Read and M. Sandström (1989). *J. Phys.: Condens. Matter*, **1**, 3459.
[71] R.D. Broadbent, G.W. Neilson and M. Sandström (1992). *J. Phys.: Condens. Matter*, **4**, 639.
[72] G.J. Herdman and G.W. Neilson (1992). *J. Phys.: Condens. Matter*, **4**, 627.
[73] M.C. Read and M. Sandström (1992). *Acta Chem. Scan*., **46**, 1177.
[74] A. Habenschuss and F.H. Spedding (1980). *J. Chem. Phys*., **73**, 442.
[75] A. Habenschuss and F.H. Spedding (1979). *J. Chem. Phys*., **70**, 3758.
[76] P.S. Salmon, G.W. Neilson and J.E. Enderby (1988). *J. Phys. C: Solid State Phys*., **21**, 1335.
[77] D.H. Powell and G.W. Neilson (1990). *J. Phys.: Condens. Matter*, **2**, 3871.
[78] N.A. Hewisch, G.W. Neilson and J.E. Enderby (1982). *Nature*, **297**, 138.
[79] D.H. Pfund, J.G. Darab, J.L. Fulton and Yanjun Ma (1994). *J. Chem. Phys*., **98**, 13102.
[80] N.T. Skipper and G.W. Neilson (1989). *J. Phys.: Condens. Matter*, **1**, 4141.
[81] J.L. Fulton, D.M. Pfund, S.L. Wallen, M. Newville, E.A. Stern, and Yanjun Ma (1996). *J. Chem. Phys*., **105**, 2161.
[82] Y. Kubozono, A. Hirano, H. Maeda, S. Kashino, S. Emura and H. Ishida (1994). *Z. Naturforsch*., **49a**, 727.